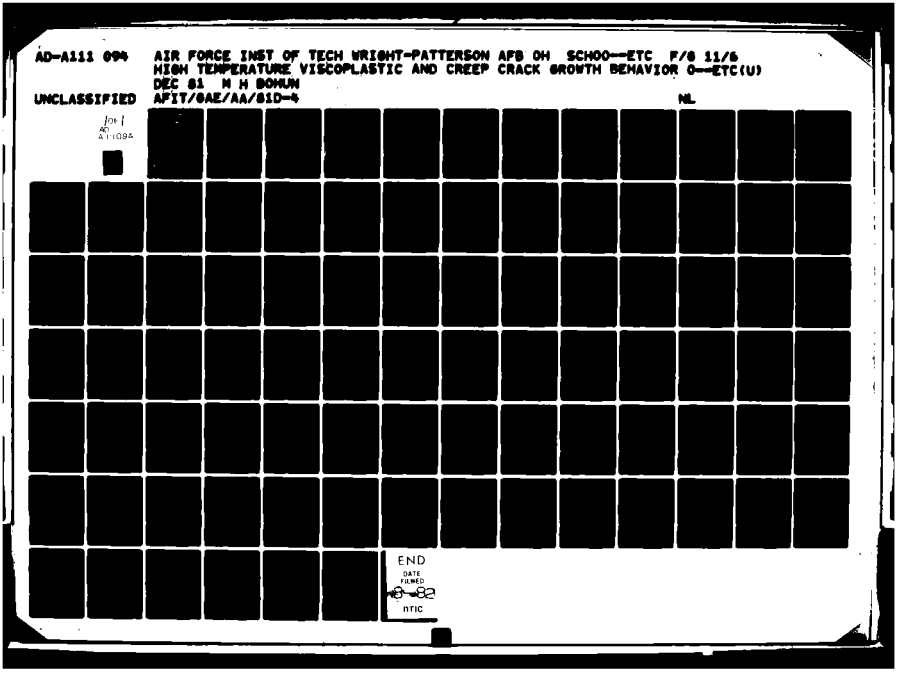
AD-A111 094
AIR FORCE INST OF TECH WRIGHT-PATTERSON AFB OH SCHOO--ETC F/G 11/6
HIGH TEMPERATURE VISCOPLASTIC AND CREEP CRACK GROWTH BEHAVIOR O--ETC(U)
DEC 81 M H BOHUN
UNCLASSIFIED
AFIT/GAE/AA/81D-4
NL
1 OF 1
AD A111094
END
DATE FILMED
82
DTIC

LEVEL II

1

AD A111094

DTIC
ELECTE
FEB 1982
S
E

DTIC FILE COPY

UNITED STATES AIR FORCE

AIR UNIVERSITY

AIR FORCE INSTITUTE OF TECHNOLOGY

Wright-Patterson Air Force Base, Ohio

82 02 18 058

AFIT/GAE/AA/81D-4

LEVEL II 1

HIGH TEMPERATURE VISCOPLASTIC AND CREEP CRACK GROWTH BEHAVIOR OF IN-100

THESIS

AFIT/GAE/AA/81D-4 Michael H. Bohun
Captain USAF

AFIT/GAE/AA/81D-4

HIGH TEMPERATURE VISCOPLASTIC AND CREEP CRACK GROWTH BEHAVIOR OF IN-100

THESIS

Presented to the Faculty of the School of Engineering

of the Air Force Institute of Technology

Air University

in Partial fulfillment of the

Requirements for the Degree of

Master of Science

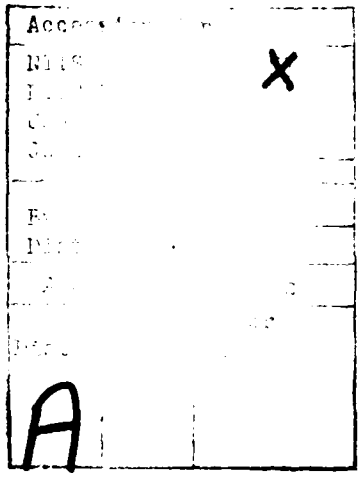

by

Michael H. Bohun

Capt USAF

Graduate Aeronautical Engineering

December 1981

ACKNOWLEDGMENTS

I would like to express my appreciation to Professor A.N. Palazotto for his guidance, advice and encouragement throughout the course of this study. Thanks go to Dr. T. Nicholas of the Air Force Materials Laboratory, for his helpful ideas, as well as sponsoring the study. Appreciation is also extended to the Materials Lab Computer Activities Group. Its manager, Robert A. Kinceses, aided in scheduling and insuring the computer program was run on a consistent basis. The technician, Miss Diane L. Delawder, aided in transfering tapes and insured CALCOMP plots were plotted accurately. Also, thanks go to Gary Griffin for his helpful instructions in incorporating MOVIE. Byu, in graphically displaying data.

I especially want to express my sincere appreciation to Miss Deborah L. Baker for her help in editing and typing of the thesis. Most of all, I want to thank the Lord for giving me the strength, endurance and patience in completing this study.

Michael H. Bohun

CONTENTS

LIST OF SYMBOLS

$\dot{(\ )}$	Time rate of change ( )
a	Half crack length in center cracked plate
(B)	Matrix relating total strain to nodal displacements
dt^i	The i^{th} time step
d_{ij}	Incremental component of total strain
d_{ij}	Incremental component of plastic strain
D_o	Bodner material constant
(D)	Elastic material matrix relating stress to total elastic strain
H	Slope of stress vs plastic strain curve
i, j	Indices
K	Stress intensity factor
K_{FE}	Stress intensity factor based on finite element model
(K)	Global elastic stiffness matrix
m	Bodner material constant
n	Bodner material constant
p	Applied load
$\{P\}$	Applied load vector
$\{Q\}$	Plastic load vector
r	Bodner material constant
S_{ij}	Deviatoric stress
t	Elapsed total time

LIST OF SYMBOLS (Continued)

W_p	Plastic strain energy density
Z	Bodner model internal state variable
Z_o, Z_1, Z_1	Bodner material constant
γ_c	Fluidity constant in Norton Creep Law
γ_p	Fluidity constant in Malvern Flow Law
ϵ	Total uniaxial strain
ϵ_{ij}	Components of total strain
ϵ_{ij}^e	Elastic components of total strain
ϵ_{ij}^p	Plastic components of total strain
ϵ_e^p	Total effective plastic strain
λ	Positive scalar constant
σ	Uniaxial stress
σ_{ij}	Components of stress
σ_e	Effective stress
$\bar{\sigma}$	Strain hardening yield stress
$\bar{\sigma}_o$	Initial yield stress
η	Material parameter, Powered Malvern
β	Material parameter, Norton Law
a	Material parameter, Exponential Malvern

ABSTRACT

IN-100, a nickel based powdered alloy, is presently used in turbine disks within the F-100 turbofan engine. It has been found that time dependent inelastic strains can be developed within this material at the high temperature environment of the turbine engine. Previous work performed by Terry D. Hinnerichs involved developing a computer program that would predict crack growth with viscoplastic flow. A large portion of his work used a strain-rate sensitive model known as the Bodner-Partom flow law. Crack growth predictions using this flow law were very encouraging, but the determination of the nine material parameters involved in the flow law presents some difficulties. Therefore, it has been proposed that a much simplified version of a strain-rate sensitive model be employed to capture viscoplastic action.

Hence, this thesis involves the study of various mathematical forms of the Malvern overstress constitutive equation. Each of these models employed a finite element computer program to predict crack growth. The computer program incorporates the constant strain triangles. The residual force method was utilized to handle variations in material stiffness due to plastic deformations and creep. In addition, a Hybrid Experimental-Numerical (HEN) procedure was used to trace crack opening displacements near the crack tip. This HEN procedure insures the model is following the experimental displacement rates accurately. Thus, the crack growth predictions are a by-product of both the rate-sensitive model and near field displacement rates.

The various mathematical representations of the Malvern model were compared to the Bodner-Partom response. Comparisons were made utilizing total plastic work generated, crack growth rates, and effective stress contours and stress profiles.

I. INTRODUCTION

BACKGROUND

Currently, the United States Air Force is very much interested in obtaining maximum service life from jet engine components. In particular, jet engine disks are being retired from service based on the failure of one in a population of 1000 turbine disks (1). Failure in these disks is considered to be a crack length of 0.03 inches. It has been determined that the remaining 999 disks have considerable residual life (approximately 80% of these retired disks have at least 10 life times remaining). Thus, a new Air Force program called Retirement-For-Cause (1, 2, 3, 4) is being initiated so that the remaining safe life of these disks can be utilized. The Retirement-For-Cause program would retire a disk component from its service life when a quantifiable crack limit has been verified through a crack inspection technique. Thus, present research in this area has focused upon crack growth prediction models. So, once a crack initiation site has been identified, the crack growth prediction model would be used to predict when the crack would reach critical size and the disk Retired-For-Cause.

In the analysis of turbine disks, their operational environment is worth noting. Various engine missions may include throttle cycling. This cycling may be due to various mission requirements such as take-off, climb, various air maneuvers, ferry, and landing. These operational aspects effect crack growth parameters such as stress and strain levels, stress intensity, and component temperature. Yet,

there are also missions in which throttle cycling is limited, therefore, engine operational parameters are constant for long periods of time called "dwell times". In this case, crack growth parameters become functions of both stress and strain levels at constant temperatures. Under these conditions, cracks in engine components under high loading cause the material to yield, forming a region of plastic deformation in which the stress-strain behavior of the material is nonlinear.

In addition to local yielding at the crack tip, high temperatures cause the material to strain without an increase in the stress level and, consequently, time dependency becomes important (this phenomenon is known as creep). These physical considerations (plastic deformation and creep with time) have been incorporated by Terry D. Hinnerichs (5) in modeling crack growth behavior of IN-100, a new nickel based powder alloy presently used in F-100 turbine disks. He developed a constant strain finite element computer program in order to model the physical behavior of the material. Inelastic behavior near the crack tip was modeled using either the Bodner-Partom or the coupled Malvern-Norton flow laws. These rate-sensitive models each differ in their constitutive development. For example, the Malvern model employs the concept of a reference stress-strain isotropic hardening function. Thus, elastic and plastic deformations are separated through the use of the Von-Mises yield criterion. The Malvern model has the advantage of a limited set of material parameters which are quite easy to determine.

A more sophisticated model, the Bodner-Partom, is based on

dislocation dynamics. In its formulation, the elastic and plastic deformations are not separated by a yield criterion. Therefore, this constitutive model is independent of the material's yield stress. The main disadvantage of the Bodner model is in its reliance upon many material constants which must be determined beforehand, and often this is not an easy task, due to coupling of the parameters.

PURPOSE

The major purpose of this thesis is to compare the Bodner-Partom flow law model with variations of the coupled Malvern overstress and Norton's Creep laws. The comparisons between the models are directed toward physical and mathematical representations of the effect on crack growth, plastic zone size, plastic stress and strain distributions, and differences in plastic work due to inelastic behavior at the crack tip. These comparisons can be used in determining if a simplified flow law, under certain restrictions, models the materials' inelastic behavior with crack growth as accurately as the sophisticated Bodner-Partom model. Thus, if one can model the plastic flow with a simplified model in which the material parameters are few and easily determined, then one has developed a useful engineering tool that can be readily used for determining plastic flow effects on crack growth. For example, the Bodner-Partom model in its present form requires, as mentioned previously, the evaluation of nine material parameters. These parameters have been evaluated for IN-100 at 1350°F based upon an experimental data set of eleven creep tests and nine tensile tests. The results of this work are published by Stouffer (6) and have been utilized by Hinnerichs,

within his finite element computer code, to model crack growth. Although the results using the Bodner expression to model crack growth are very encouraging, determination of Bodner's nine material parameters are difficult, and require a thorough understanding of the model's development. Therefore, it has been proposed that a simplified flow law with two material constants, such as the coupled Malvern/Norton, could provide the necessary plastic flow required to accurately model the plastic zone at the crack tip.

Hinnerichs (5) compared effective stress and strain at the crack tip using both the Bodner-Partom and the linear Malvern-Norton models. Results showed good correlations between the two models, even though the linear Malvern model had a limited range in predicting the plastic strain-rate. Consequently, the focus of this thesis will be toward the development of variations of the coupled Malvern-Norton model to capture the full variation of plastic strain rates over a range of stress levels. These rate-sensitive models will then be incorporated into the computer program developed by Hinnerichs. Also, the finite element program will be used to model crack growth based on the new variations of the coupled Malvern-Norton model and compare crack growth behavior to the response using the Bodner-Partom model.

GENERAL APPROACH

A two-dimensional (constant strain triangle) finite element program developed by Terry D. Hinnerichs at AFIT will be used to study the effects of various viscoplastic flow laws on crack growth.

Initially, different forms of the Malvern overstress flow law will be studied. These forms will include linear, power, and exponential mathematical expressions of the constitutive laws. Comparisons of these different forms will be made with each other and to experimental tensile tests for IN-100.

The Malvern law will then be superimposed upon the secondary creep Norton flow law to express a unified flow law. This unified flow law approach has been proposed by Zienkiewicz and Cormeau (7), and will be used with the linear, power, and exponential forms of the Malvern equation (these forms will be called the coupled forms).

In addition to these coupled forms, a form using only the exponential form of the Malvern equation will be used to fit the range of plastic strain rates (this form will be called the uncoupled form). This new modification couples the viscoplastic and creep strains together without the superposition technique, as mentioned above.

Once good correlations among stress, strain, and strain rate behavior of these models have been made, then each of these strain-rate sensitive models will be incorporated into the finite element analysis of crack growth.

The crack growth model consists of a center cracked plate specimen in which constant strain triangles are used to model the plate. Element size has been reduced near the crack tip with element refinements in the order of a grain size for IN-100.

Crack-opening displacements from experimental data obtained by W. Sharpe (8) has been utilized within the computer code so that crack

opening displacements (COD) will accurately model the actual experimental displacement versus time relations. For example, if the C.O.D. in the Sharpe data curve exceeds the finite element calculated displacement, then a node at the crack tip is released so that the correct C.O.D. versus time can be matched. Thus, predicted crack length versus time becomes a by-product of C.O.D.

In the analysis of crack growth using the center crack plate, two different applied load levels have been incorporated. One load level of 10896 lbs. with a stress intensity factor, K, of 25 KSI$\sqrt{in}$, and another load level of 16060 lbs. with a K of 36.8 KSI$\sqrt{in}$ are considered. Each load case uses both the Bodner-Partom and coupled Malvern-Norton equations to model the effects of time dependent plasticity on crack growth.

ASSUMPTIONS

Basic assumptions used in the formulation of strain-rate sensitive constitutive models are as follows:

1. The total strain within a material may be decomposed into elastic and plastic components. This assumption is computationally convenient since the finite element code formulates an elastic stiffness matrix directly, while effects of plasticity can be incremented separately by a rate-sensitive model via the residual force method (see theory section). This eliminates the need to modify the elastic stiffness matrix.
2. Plastic incompressibility is assumed such that hydrostatic (spherical) stress has no effect on the yield behavior of the

material.

3. The formulation of both Malvern's and Bodner's flow laws implies that plastic strain rates are linearly related to stress rates.

4. The material's behavior is considered isotropic up to the elastic limit. After exceeding the yield point, two different hardening rules are enforced depending on the constitutive flow law used. The Malvern-Norton combination assumes isotropic hardening. Thus, the yield surface expands uniformly with respect to the hydrostatic stress line. On the other hand, the Bodner-Partom Model uses a kinematic hardening function which can vary the material's hardness through the use of a recovery term. If the recovery term is not included, the Bodner's law follows the isotropic hardening rule (9).

5. Malvern's constitutive model assumes the existence of an initial yield surface. This surface is traced through time by the model and defines the point at which plasticity occurs. On the contrary, Bodner's flow law was developed independent of a yield surface and, thus, traces plastic strain from the start of load application.

II. VISCOPLASTICITY AND CREEP THEORY

A rheological model for the Malvern-Norton stress-strain relationship may be represented by the total strain behavior of a material as shown in Figure 1

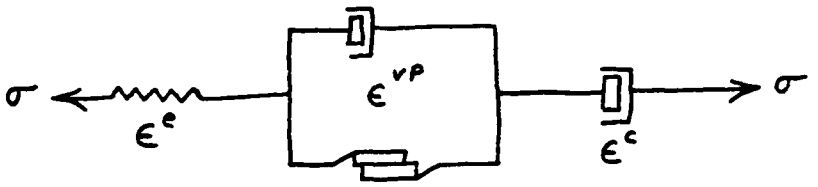

FIGURE 1.

The total strain is composed of both elastic (represented by the spring) and inelastic strains (slides and dashpots). The inelastic strain is made up of the time dependent viscoplastic strain as well as the creep strain. The viscoplastic strain occurs only when the yield point of the material is exceeded and is considered nonrecoverable. Thus, the slides can move in only one direction. Another time dependent strain called creep strain (represented by the second dashpot), is an inelastic strain that continuously forms throughout time and is independent of the initial yield stress.

Thus, the total strain using tensor notation is

$$\epsilon_{ij}^{TOTAL} = \epsilon_{ij}^{elastic} + \epsilon_{ij}^{plastic} \tag{2.1}$$

where $\epsilon_{ij}^{p} = \epsilon_{ij}^{vp} + \epsilon^{c}$, is the total plastic response including both viscoplasticity and creep strains (10,11,12).

These strains can be expressed in rate dependent form as

$$\dot{\epsilon}_{ij}^{Total} = \dot{\epsilon}_{ij}^{Elastic} + \dot{\epsilon}_{ij}^{Plastic} \quad \text{where } \dot{\epsilon} = \frac{d\epsilon}{dt} \tag{2.2}$$

Therefore, the total strain rate is composed of both the elastic strain rate, which is related to stress by the derivative of Hooke's law, and the plastic strain rate.

The plastic strain rate is related to stress by the Prandtl-Reuss equation. This equation assumes, as mentioned previously, that an increment of plastic strain is proportional to the instantaneous deviatoric stress. The deviatoric stress represents the radius of the Von-Mises yield cylinder in 3-D stress space. The Von-Mises yield surface, represented in three-dimensional stress space, is shown in Figure 2

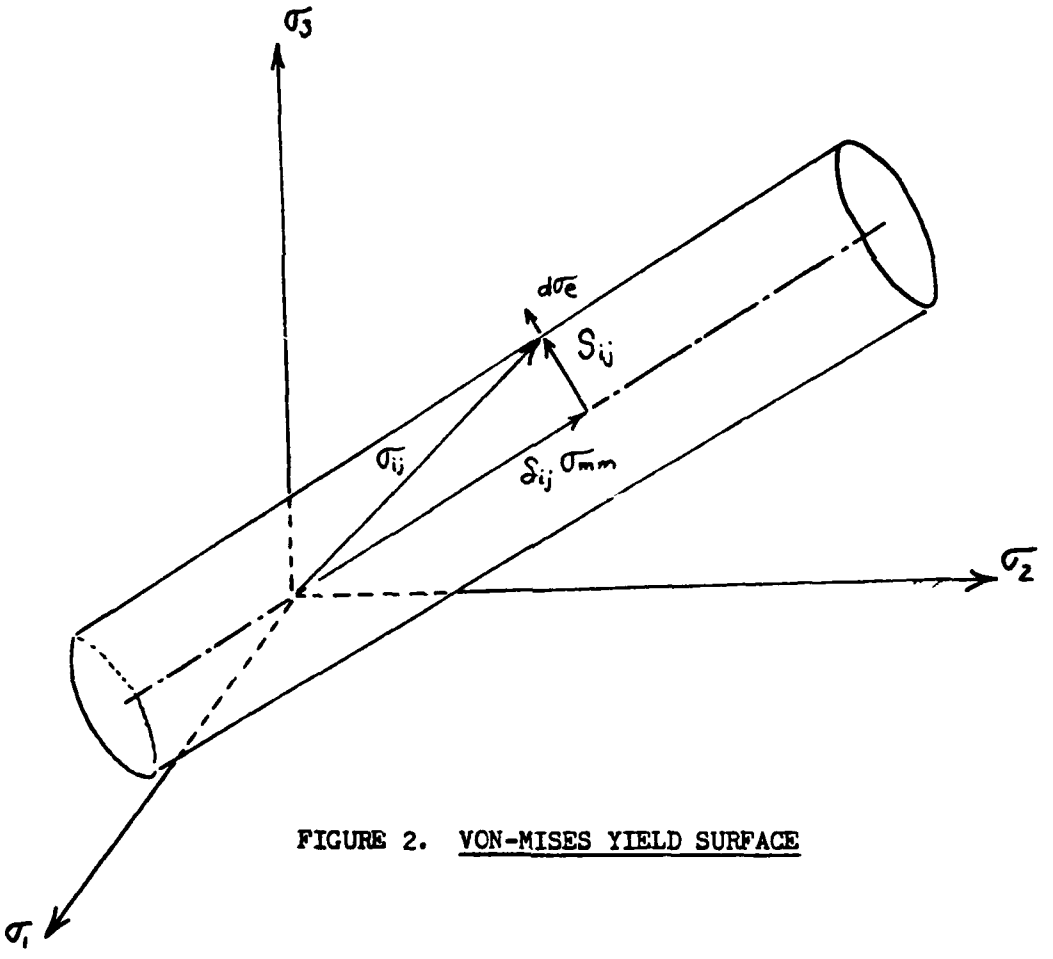

FIGURE 2. VON-MISES YIELD SURFACE

where, from Figure 2, S_{ij} is the deviatoric stress vector, σ_{ij} is the total stress vector, and $\delta_{ij}\sigma_{mm}$ is the hydrostatic stress vector which lies on the line where $\sigma_{11} = \sigma_{22} = \sigma_{33} = 0$ (13).

The Von-Mises yield criteria implies that if a state of stress lies on the yield surface, then plastic flow occurs. If, however, the state of stress decreases and lies within the cylinder, elastic strains occur. The Von-Mises yield surface extends to infinity parallel to the cylindrical axis shown in Figure 2. During plastic straining, this surface expands normal to itself, and thus, isotropic hardening is enforced within the plastic zone.

The Prandtl-Reuss Equation takes the form

$$\dot{\epsilon}_{ij}^{P} = \lambda S_{ij} \tag{2.3}$$

where S_{ij} represents the radius of the yield cylinder in 3-D stress space. The λ parameter is a material behavior value expressing the material's plastic flow response. This plastic flow response can be represented by several well-known flow laws, one of which is the Malvern Linear Overstress law (15). This law accounts for viscoplasticity during an incremental change in the stress level (overstress) and is represented constitutively by

$$\dot{\epsilon}_{ij}^{P} = \gamma_P \left[\frac{\sigma_e}{\bar{\sigma}(\epsilon_e^P)} - 1 \right] \frac{3}{2} \frac{S_{ij}}{\sigma_e} \tag{2.4}$$

The parameter γ_p is the fluidity constant which can be varied to match the material's strain-rate sensitivity. The effective stress, σ_e , is a stress invariant which measures the incremental change of the yield surface due to an overstress. The deviatoric stress, S_{ij} , represents a point at which plasticity is measured. The strain hardening yield stress function, $\bar{\sigma}(\epsilon_e^p)$, is a function of the effective plastic strain and is used as a universal stress-strain curve that governs the material's uniaxial inelastic behavior during loading. This function takes the form (assuming a linear strain hardening over a given uniaxial stress-strain segment)

$$\bar{\sigma}(\epsilon_e^p) = \bar{\sigma}_o + H' \epsilon_e^p \qquad (2.5)$$

where $\bar{\sigma}_o$ is the material's initial yield stress, H' represents the slope of the uniaxial stress-strain curve and ϵ_e^p is the effective plastic strain (14).

The strain hardening yield stress function is valid only when used with monotonically increasing loads. This equation is based on the Von-Mises yield criterion modeling isotropic hardening and does not account for the Baushinger effects that occur during load reversal.

The flow law that is coupled to the Malvern is the Norton law for secondary creep. This law accounts for long term creep strains that occur with time. The creep response for all practical purposes can be considered negligible, since crack growth studies considered herein were at high levels of strain rates for relatively short periods of time, but this phenomenon will be included for completeness.

Norton's Creep law (11) is expressed in multiaxial form as

$$\dot{\epsilon}_{ij}^{p} = \gamma_c \left(\sigma_e\right)^{\beta} \frac{3}{2} \frac{S_{ij}}{\sigma_e} \qquad (2.6)$$

where γ_c and β are material constants to be determined from uniaxial creep test results. See Appendix A for determination of these values.

The coupling of Malvern's overstress law with Norton's secondary creep law has been proposed by Zienkiewicz and Cormeau (4). The coupled form would represent a unified flow law where both visco-plastic and creep strains are superimposed to form a total plastic strain.

The interest of the next section is to to examine some of the parameters presented previously and discuss their individual characteristics.

CONSTITUTIVE MALVERN MODEL DEVELOPMENT

The simplest form of the Malvern law has been shown in Equation (2.4). It has one material parameter, γ_p , which models plastic strain-rate sensitivity. Thus, a value for γ_p must be chosen to fit the strain-rate required for the analysis. Hence, for the simpliest form or so-called linear model, determination of γ_p is highly problem dependent. For example, in the case of plastic flow near a crack tip or geometrical discontinuity, both magnitudes of strain-rate and stress levels are high. Also, as one traverses across the plastic zone ahead of the discontinuity, stress and strain rate levels vary. Thus, if one is attempting to capture these variations within the plastic zone, using a one parameter function such as the Malvern equation, an averaging technique must be used. Also, the value of γ_p is chosen high enough so that the linear model will

predict the proper plastic flow at both high and low stress intensity factor levels.

To eliminate the problem dependency that the linear Malvern model presents in predicting a range of strain rates, other versions of the Malvern constitutive equations are introduced.

MALVERN'S POWER LAW. The power version can be expressed in multiaxial form as

$$\dot{\epsilon}_{ij}^{P} = \gamma_P \left[\frac{\sigma_e}{\bar{\sigma}(\epsilon_e^P)} - 1 \right]^{\eta} \frac{3}{2} \frac{S_{ij}}{\sigma_e} \qquad (2.7)$$

where $\bar{\sigma}(\epsilon_e^P)$ is a function discussed in a subsequent section, but for completeness, the reader can think of it as the plastic stress-strain curve. The parameters γ_P and η are introduced to establish material dependency rather than problem dependency. These two material constants are determined by taking the natural logarithm of each side of the above equation, then selecting two experimental strain rates and their corresponding stress levels. This establishes two equations which can be used to find γ_P and η . The power form of the Malvern law predicts only two experimental strain rates accurately. These results will be graphically shown in the experimental response section.

EXPONENTIAL MALVERN. Another form of the Malvern flow law uses an exponential mathematical expression. This form of the governing constitutive equation has been used in the analysis of propagation of plastic waves of uniaxial stress in long rods and bars (16) and

expressed as

$$\dot{\epsilon}_{ij}^{p} = \gamma_p \left\{ \exp\left(\frac{\sigma_e - \bar{\sigma}(\epsilon_e^p)}{a} \right) - 1 \right\} \frac{3}{2} \frac{S_{ij}}{\sigma_e} \qquad (2.8)$$

The parameters γ_p and a characterize the shape and, therefore, rate sensitivity of the strain-rate versus stress curve, and the calculations for their determination can be found in Appendix B. The term $(\sigma_e - \bar{\sigma}(\epsilon_e^p))$ is called the overstress, where, in the uniaxial case, the effective stress, σ_e , reduces to an applied stress and the strain hardening yield stress value, $\bar{\sigma}(\epsilon_e^p)$ characterizes the viscoplastic nonlinear response of the material's uniaxially stress-strain curve (see Figure 3).

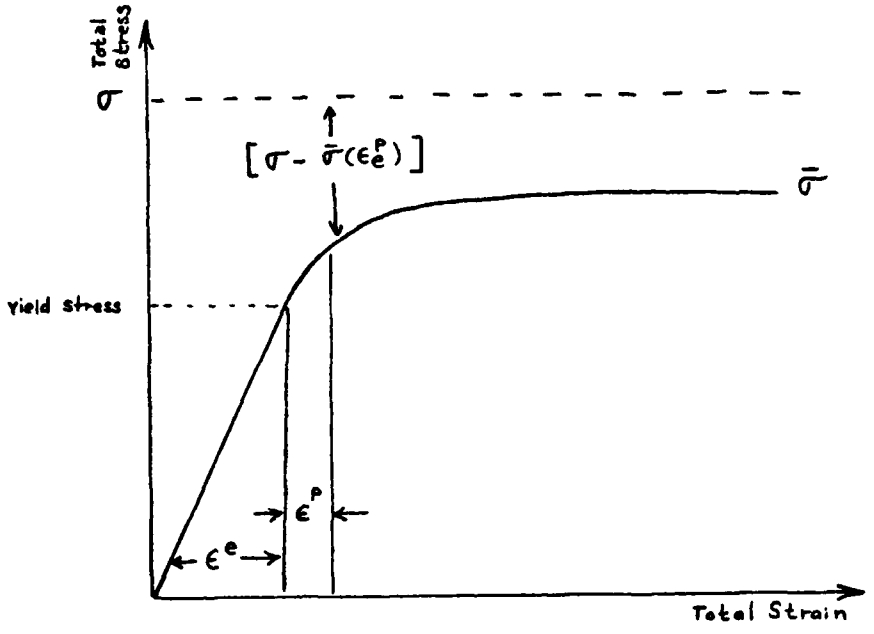

FIGURE 3. UNIAXIAL STRESS-STRAIN CURVE SHOWING OVERSTRESS

The exponential form has been found to match experimental strain rates over a range of corresponding stress levels (see section III for these results). Hence, as noted in the experimental section, the exponential form of the Malvern law is the most accurate of all versions in predicting actual material behavior.

BODNER-PARTOM CONSTITUTIVE MODEL

The Bodner-Partom constitutive equation expressed in uniaxial form is

$$\dot{\epsilon}^p = \frac{2}{\sqrt{3}} D_o \exp\left\{-\frac{1}{2}\left(\frac{Z}{\sigma}\right)^{2n}\frac{n+1}{n}\right\} \qquad (2.9)$$

where Z represents the macroscopic measure of hardness; n is a constant controlling the strain-rate sensitivity; and D_o expresses the limiting value of strain rate. A detailed discussion of these constitutive model parameters is presented in a technical report by Stouffer (6,17). Hinnerichs (5) explains the details of how Bodner's flow law is numerically integrated in the finite element program used herein. It should be noted that this material model is capable of handling unloading or cyclic loading with a more physically correct description than Malvern's model.

Table 2.1 shows a list of the current coefficients developed by Stouffer (6) for IN-100 at 1350 F. These nine constants, although not all shown in Eq (2.10), are used in the total response of the Bodner-Partom flow law to calculate plasticity within the finite element program.

TABLE 2.1

COEFFICIENTS FOR IN-100 AT 1350 F

Material Parameter	Description	Value
E	Elastic modulus	21.3×10^3 KSI
n	Strain rate exponent	0.7
D_0	Limiting value of strain rate	10^4 sec
Z_0	Limiting value of hardness	915.0 KSI
Z_1	Maximum value of hardness	1015.0 KSI
Z_2	Minimum value of hardness	600.0 KSI
m	Hardening rate exponent	2.57 KSI^{-1}
A	Hardening recovery coefficient	1.9×10^{-3} sec^{-1}
r	Hardening recovery exponent	2.66

III. EXPERIMENTAL RESPONSE OF IN-100 AT 1350°F

In a technical report by Stouffer (6), the results of twenty mechanical tests performed on IN-100 are tabulated and graphically displayed. Eight of these tests were tensile in which the control variable was strain rate and the observed variable was stress. Eleven of the tests were designated creep, in which the control variable was stress and the observed variable was strain rate. The stable values of stress and strain rate from these experiments were plotted. The results show a linear response (see Figure 4). If a best line fit is made to the data, the slope of the creep response is smaller than the tensile. Thus, if one wants to differentiate between creep and viscoplasticity, the break point (yield point) is the point in which the slope changes, and for the subsequent figures it has been chosen to be 125 KSI. The idea of differentiation between plasticity and creep fits the formulation of the coupled Malvern-Norton flow law combination. Therefore, the Norton law is matched to the lower sloped creep data tests, while the coupled Malvern-Norton combination is matched to the higher sloped tensile tests.

COUPLED LINEAR MALVERN RESPONSE. Figure 5 shows the calculated response of the coupled linear Malvern-Norton flow law. The experimental strain rates below 10^{-5} sec^{-1} designate creep strains and have been calculated using the uniaxial form of Norton's secondary creep law as shown in Eq 3.1

$$\dot{\epsilon}^{p} = \gamma_c (\sigma)^{\beta} \qquad (3.1)$$

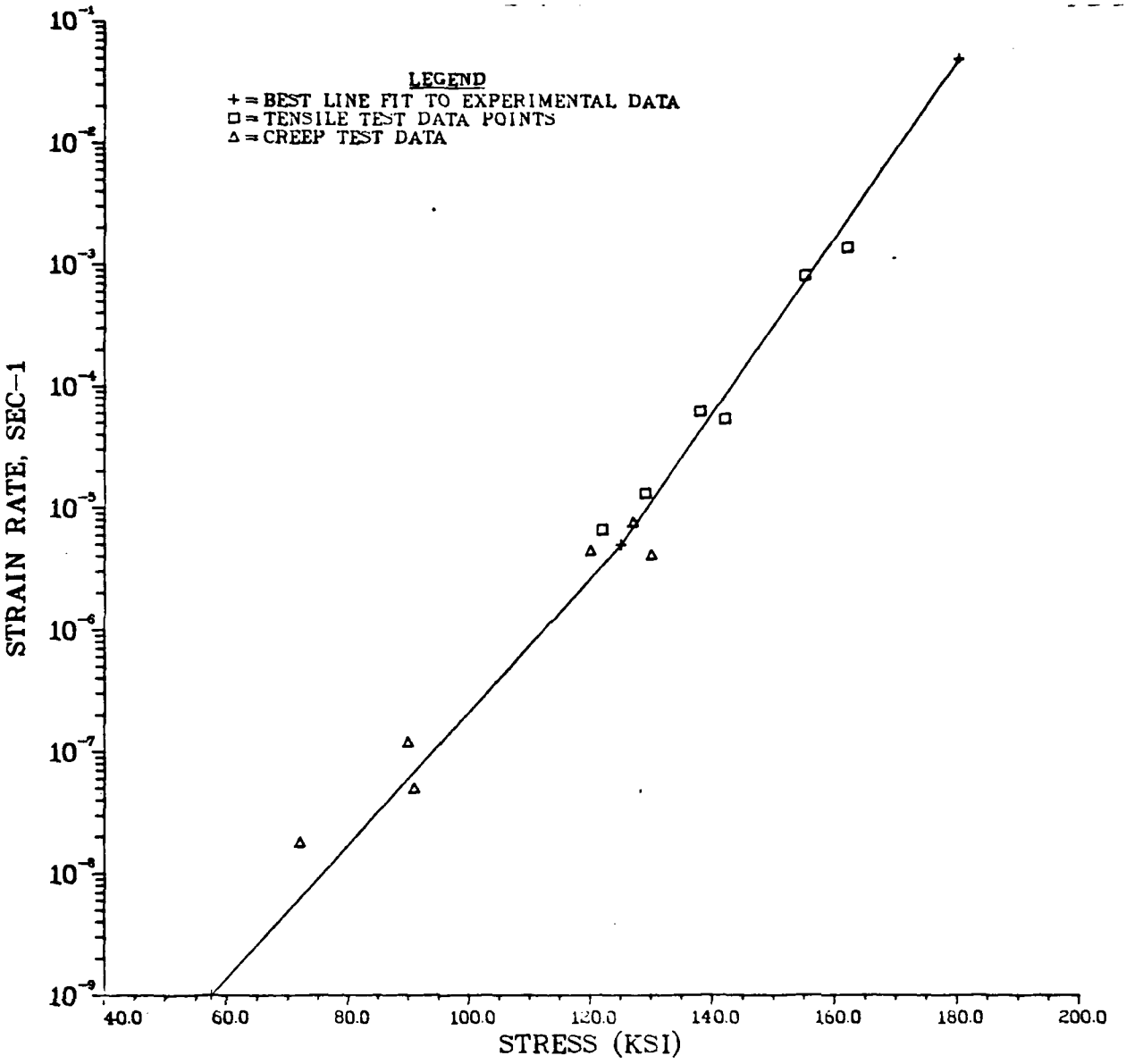

FIGURE 4. EXPERIMENTAL VALUES OF STRAIN RATE VERSES STRESS FROM TENSILE AND CREEP RESPONSE OF IN100 AT 1350F.

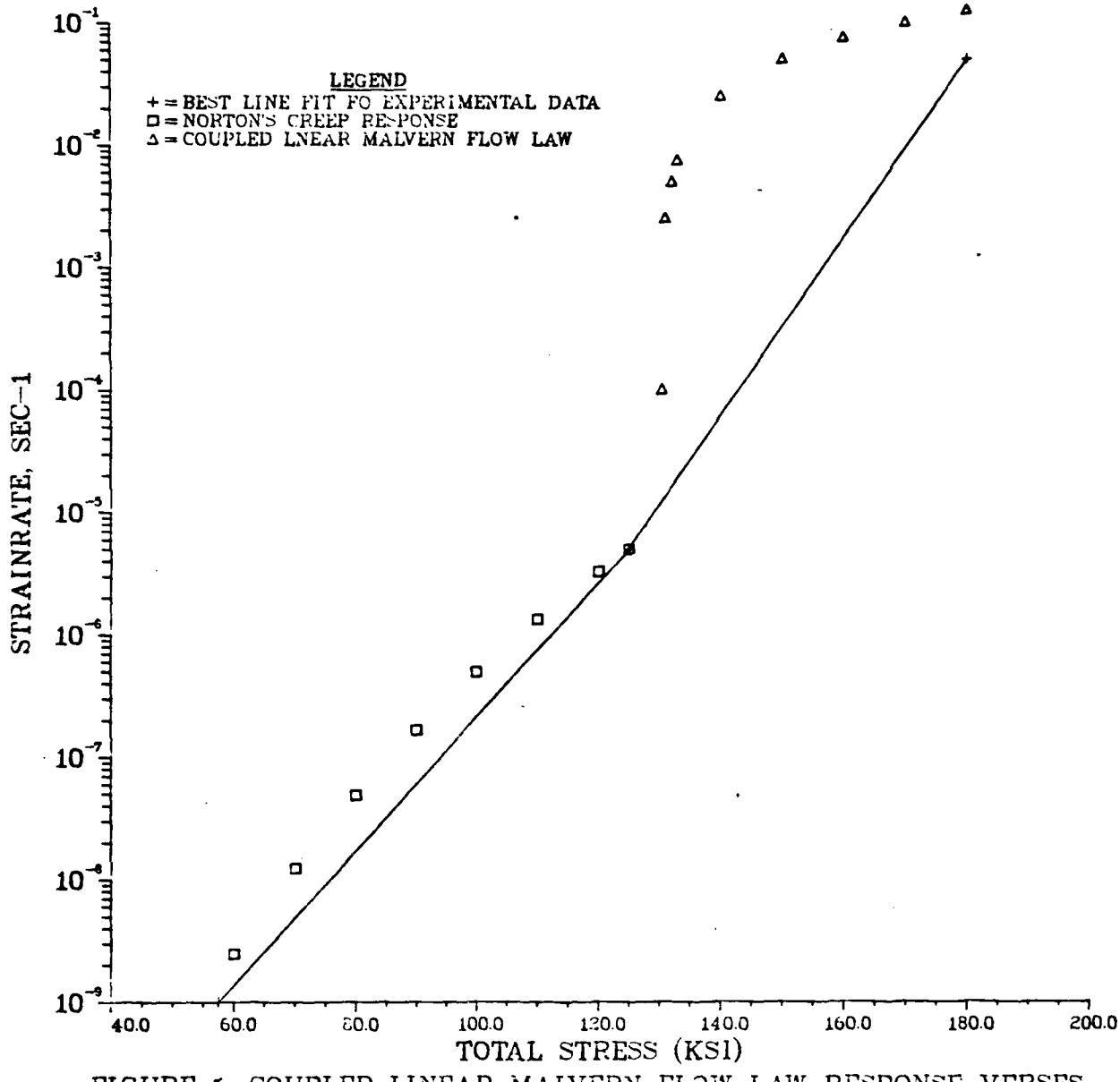

FIGURE 5. COUPLED LINEAR MALVERN FLOW LAW RESPONSE VERSES EXPERIMENTAL VALUES OF STRAIN RATE FOR IN100 AT 1350F.

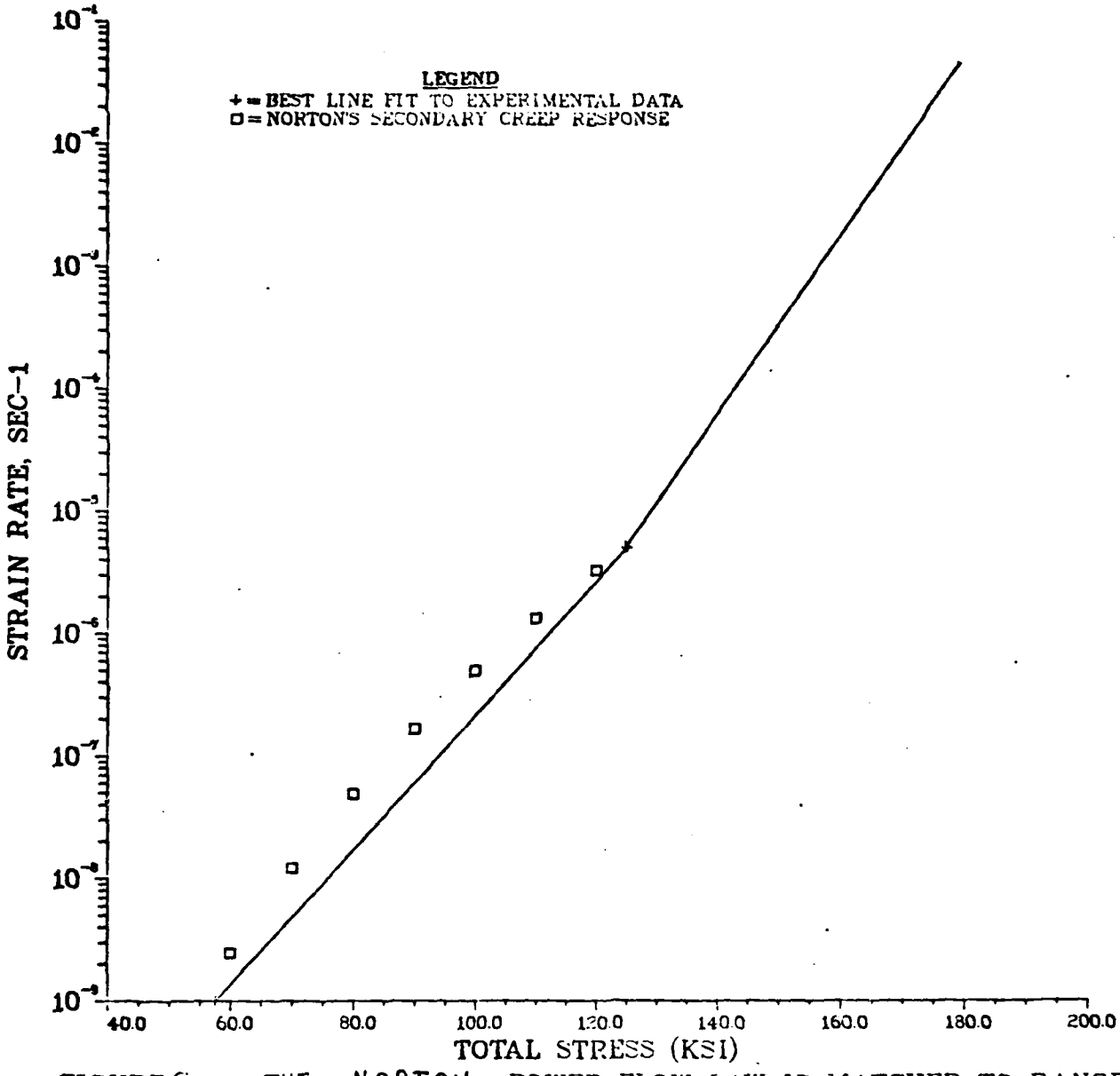

FIGURE 6. THE NORTON - POWER FLOW LAW IS MATCHED TO RANGE OF TOTAL STRAIN RATE FOR IN100 AT 1350F.

For the calculated response, fixed material constants of γ_c equals $8.7953 \times 10^{-28}/\text{KSI}^{10.3747}$ sec and β equals 10.3747 were used (determination of these constants are discussed in Appendix A). Substituting the above parameters and stress values ranging from 61 to 125 KSI, the calculated response of Equation 3.1 is determined. This power law function, observed in Figure 6 shows good correlation to the best line fit of experimental data in the creep strain region.

The experimental tensile tests at high stable strain rates (10^{-5} sec^{-1} or greater) are matched with the viscoplastic response of the coupled linear Malvern equation expressed in multiaxial form as

$$\dot{\epsilon}_{ij}^{p} = \gamma_p \left[\frac{\sigma_e}{\bar{\sigma}(\epsilon_e^p)} - 1 \right] \frac{3}{2} \frac{S_{ij}}{\sigma_e} + \gamma_c (\sigma_e)^{\beta} \frac{3}{2} \frac{S_{ij}}{\sigma_e} \qquad (3.2)$$

For the calculated response, the uniaxial form of Eq 3.3 is used

$$\dot{\epsilon}^{p} = \gamma_p \left[\frac{\sigma}{\bar{\sigma}} - 1 \right] + \gamma_c (\sigma)^{\beta} \quad \text{if } \sigma > \bar{\sigma} \qquad (3.3)$$

where $\bar{\sigma}$ =125 KSI is the perfectly plastic yield stress value, and γ_p =.33 sec^{-1} was chosen to match the expected average problem dependent strain rate for the fracture mechanics problem which is discussed in section V. Using the above parameters and stress values ranging from 60 to 180 KSI, the calculated response of Eq 3.3 can be determined. Figure 7 shows that this coupled response matches only one experimental strain rate accurately, while variations above or below

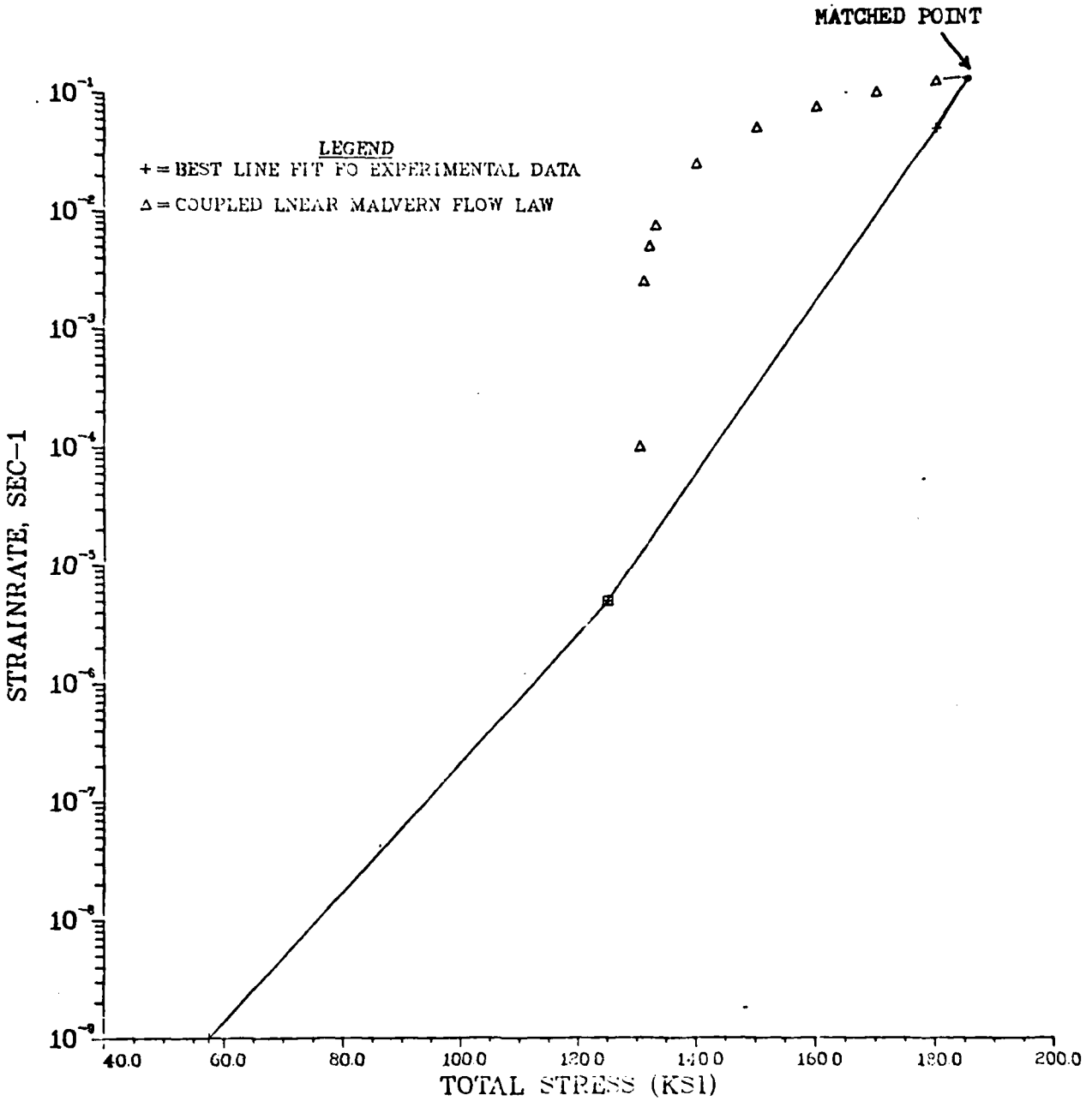

FIGURE7 . COUPLED LINEAR MALVERN FLOW LAW RESPONSE VERSES EXPERIMENTAL VALUES OF STRAIN RATE FOR IN100 AT 1350F.

the "matched point" will be in error. Therefore, the coupled linear Malvern expression, in this highly problem dependent form, is not useful in predicting any variations in plastic strain rates.

The following sections will introduce different forms of the Malvern expression containing material parameters which constitute material dependency rather than problem dependency.

MALVERN'S COUPLED POWER RESPONSE. The next version of the Malvern-Norton combination is the power law form, expressed uniaxially as

$$\dot{\epsilon}^{p} = \gamma_p \left[\frac{\sigma}{\bar{\sigma}} - 1 \right]^{\eta}_{+} + \gamma_c (\sigma)^{\beta} \quad \text{if } \sigma > \bar{\sigma} \qquad (3.4)$$

The parameters $\gamma_p = 0.3236$ sec^{-1} and $\eta = 2.2746$ have been determined from the experimental data as discussed in Appendix B. The values of γ_c, β and $\bar{\sigma}$ have been previously determined and thus, Equation 3.4 becomes a function of the stress level. Inserting values of stress, corresponding values of plastic strain rates are determined and then plotted in Figure 8. The coupled Malvern power response at the levels of 10^{-5} sec or greater match only two experimental strain rates accurately. Thus, Malvern's power law, although in material dependent form, is limited in predicting the total range of experimental strain rates.

MALVERN'S COUPLED EXPONENTIAL RESPONSE. The next constitutive equation is in exponential form and represented uniaxially as

$$\dot{\epsilon}^{p} = \gamma_p \left\{ \exp\left(\frac{\sigma - \bar{\sigma}}{a} \right) - 1 \right\} + \gamma_c (\sigma)^{\beta} \quad \text{if } \sigma > \bar{\sigma} \qquad (3.5)$$

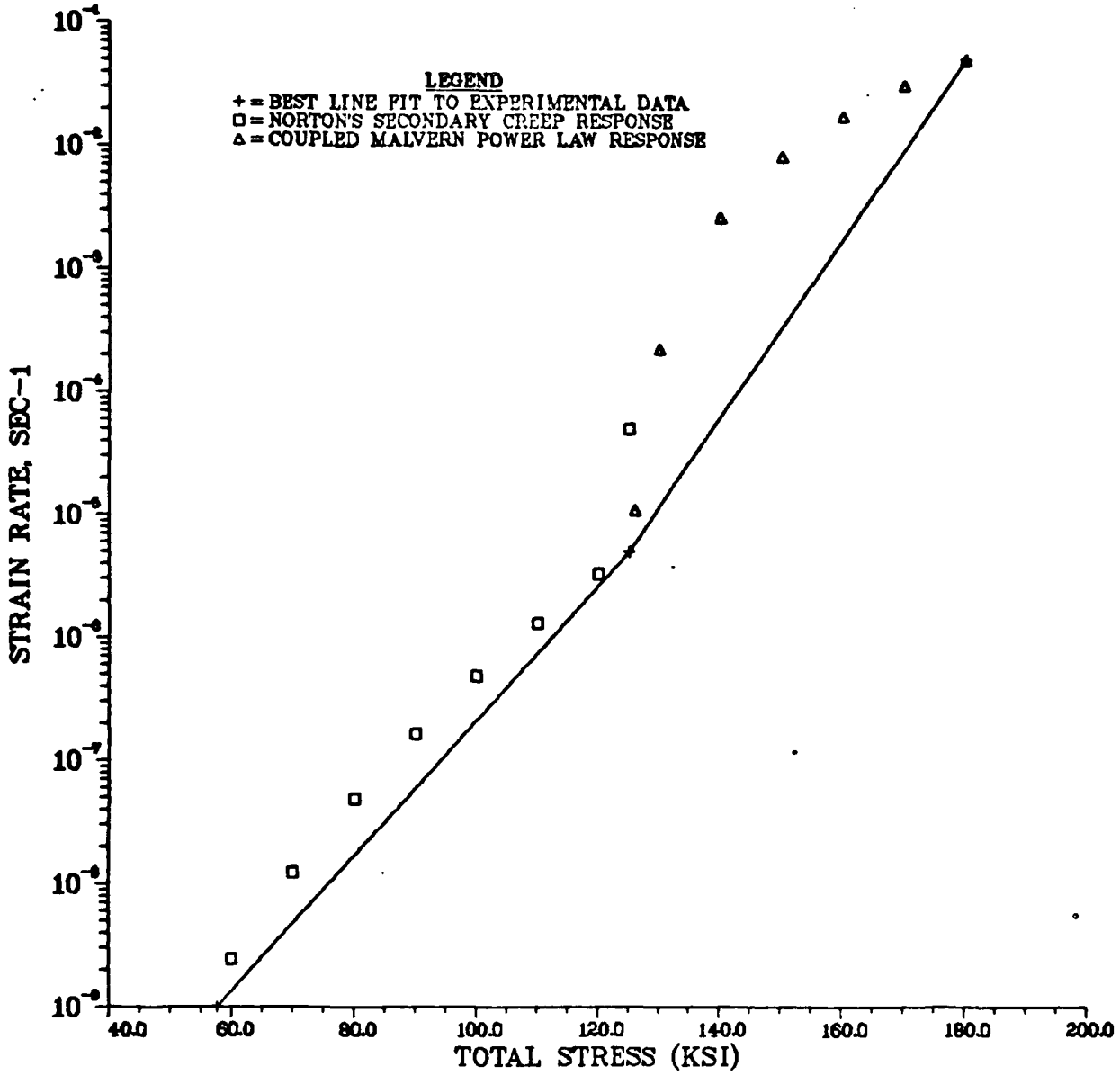

FIGURE 8. COUPLED MALVERN POWER FLOW LAW IS MATCHED TO RANGE OF TOTAL STRAIN RATE FOR IN100 AT 1350F.

The determination of γ_p and a are shown in Appendix B, while the values of the parameters γ_c, β and $\bar{\sigma}$ have been previously introduced. Taking $\gamma_p = 4.3289 \times 10^{-6}$ sec^{-1} and $a = 5.9716$ and substituting these values into Eq 3.5, the calculated response can be easily determined by substituting stress values ranging from 61 KSI-180 KSI. The results of these calculations are shown in Figure 9, indicating that the exponential form matches the high experimental strain rates very accurately.

MALVERN'S UNCOUPLED EXPONENTIAL RESPONSE. The uncoupled exponential constitutive equation does not include Norton's law for secondary creep and is expressed uniaxially as

$$\dot{\epsilon}^p = \gamma_p \left\{ \exp\left(\frac{\sigma - \bar{\sigma}}{a} \right) - 1 \right\} \quad \text{if } \sigma > \bar{\sigma} \qquad (3.6)$$

The parameters γ_p and a are material constants which capture the material's strain rate sensitivity over the entire range of plastic strain rates. Thus, the value of $\bar{\sigma} = 61$ KSI was set at the lowest strain rate measured experimentally, so that all rates above this level may constitute viscoplastic strain rates. The calculated response, shown in Figure 10, is determined by substituting $\gamma_p = 9.5382 \times 10^{-10}$ sec^{-1} and $a = 7.0767$ (see Appendix B for their determination) and stress values ranging from 61 KSI-180 KSI. It is interesting to note that the expressions used in Eq 3.6 give very close results with the experimental, since one tries to develop the γ_p and a to depict a total range of stress greater than $\bar{\sigma} = 61$ KSI. Equation 3.5 also states the exponential Malvern function, incorporating γ_p and a parameters which adjust the

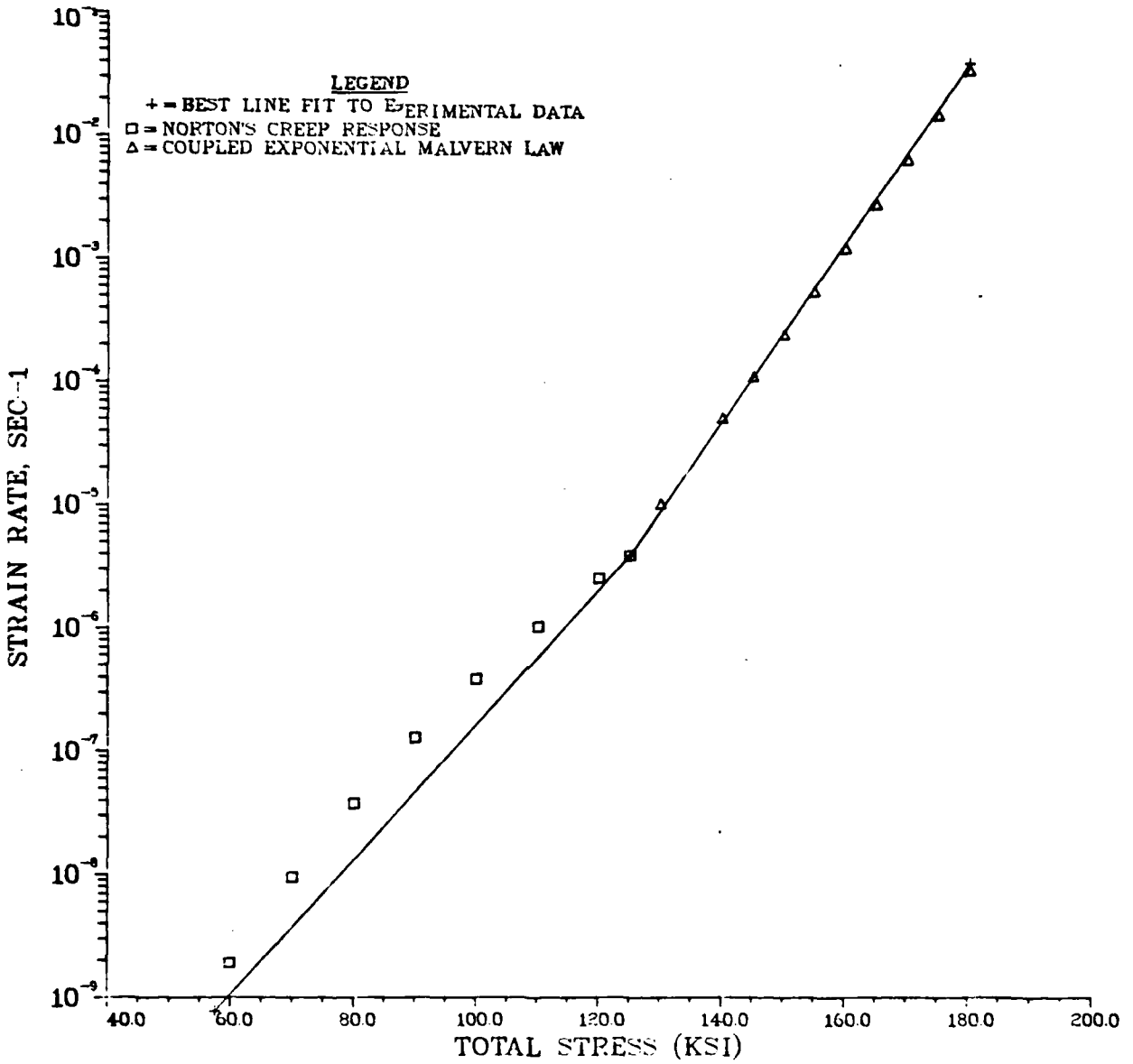

FIGURE 9 . COUPLED EXPONENTIAL MALVERN FLOW LAW IS MATCHED TO RANGE OF TOTAL STRAIN RATE FOR IN100 AT 1350F.

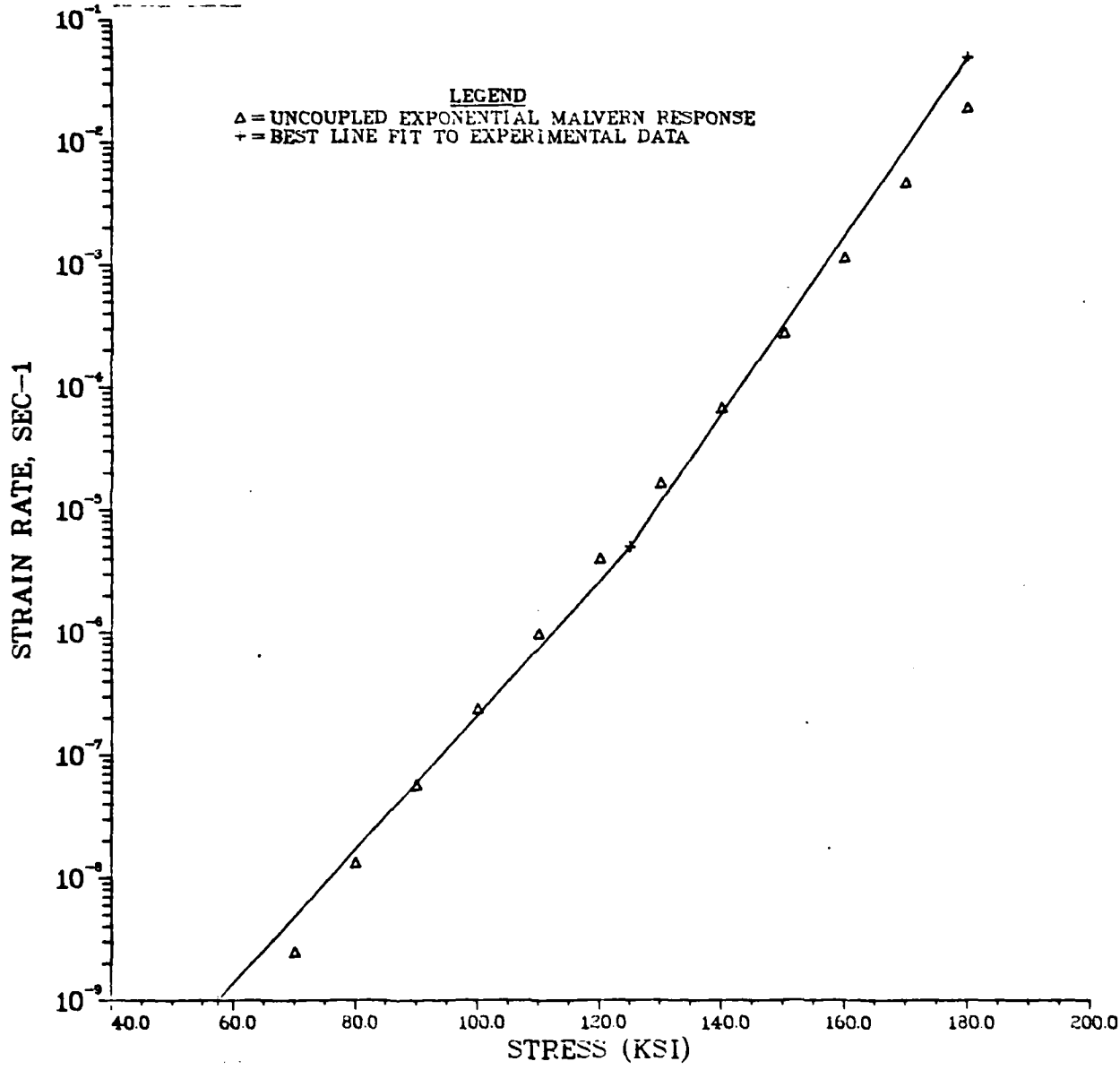

FIGURE 10. UNCOUPLED MALVERN EXPONENTIAL FLOW LAW IS MATCHED TO RANGE OF TOTAL STRAIN RATES FOR IN100 AT 1350F.

model's strain rate sensitivity if stress is greater than $\bar{\sigma}$ =125 KSI. Thus, by using the exponential form, one can arbitrarily set the $\bar{\sigma}$ value and corresponding γ_ρ and a expressions to match the range of experimental strain rates of interest.

Upon the examination of the various versions of the Malvern model, it has been determined that the exponential constitutive Malvern equation predicts experimental strain rates with the most accuracy. Malvern's power form, although material dependent, predicts only two experimental strain rates, while the linear Malvern predicts only one strain rate and is highly problem dependent.

IV. THE YIELD STRESS FUNCTION AND FINITE ELEMENT APPLICATIONS

The strain hardening yield stress function is an equation which is used in all versions of the Malvern overstress flow law. This function represents the material's nonlinear behavior based on uniaxial tensile tests. For example, three of Stouffer's (6) eight strain rate controlled tests on IN-100 are shown in Figure 11. The general shape of these curves is quite uniform throughout the range of strain rates (providing no stress recovery is occurring). Thus, it is assumed that a universal strain hardening yield stress function may be chosen to represent the entire range of the material's nonlinear behavior. To develop this expression, a multilinear fit is performed to one experimental tensile curve. For numerical purposes, the equation is developed as a function of plastic strain and used within the finite element code for time integration of the Malvern flow law (integration performed by Euler linear extrapolation).

The strain hardening yield stress function can be expressed in general form as

$$\bar{\sigma}(\epsilon_e^p) = \bar{\sigma}_o + H' \epsilon_e^p \qquad (4.1)$$

where $\bar{\sigma}_o$ is the initial value of yield stress, H' is the plastic slope of the stress-strain curve and ϵ_e^p is the effective plastic strain.

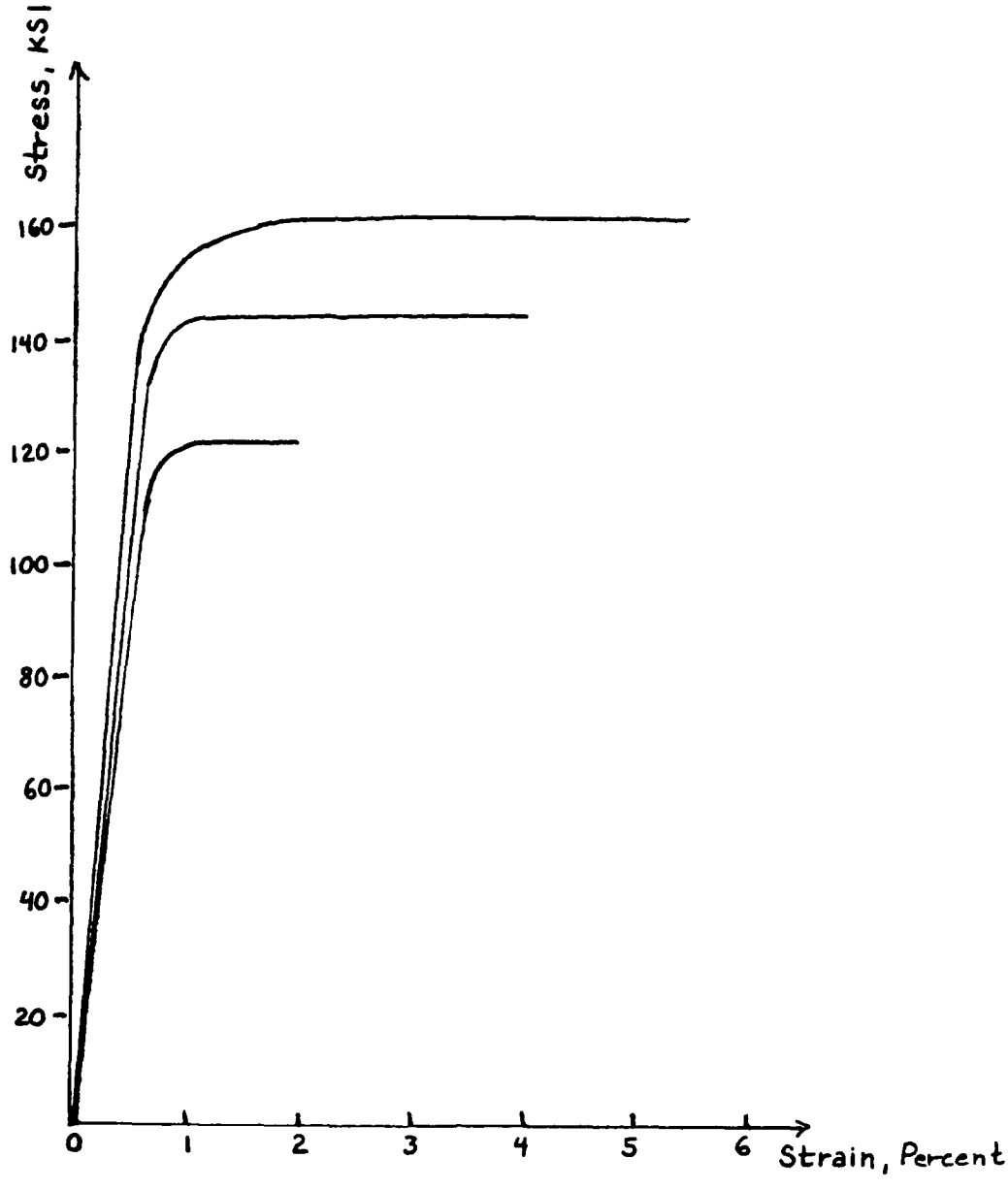

FIGURE 11. TENSILE RESPONSE OF IN-100 AT 1350°F

This function is used within the Malvern flow law to express an overstress ratio, $\frac{\sigma_e}{\bar{\sigma}}$. The magnitude of this ratio determines the incremental strain rate produced with time. For example, the time integration of the Malvern flow law is as follows (the superscript, n, refers to the iteration number)

$$\left\{\dot{\epsilon}_{ij}^{p}\right\}^{n} = \begin{cases} 0 & \text{if } \sigma_e^{n-1} < \bar{\sigma}(\epsilon_e^p)^{n-1} \text{ and } \sigma_e^{n-1} > \sigma_e^{n} \\ \gamma_p\left[\dfrac{\sigma_e^{n-1}}{\bar{\sigma}(\epsilon_e^p)^{n-1}} - 1\right]\dfrac{3}{2}\dfrac{S_{ij}^{n-1}}{\sigma_e^{n-1}} & \text{if } \sigma_e^{n-1} > \bar{\sigma}(\epsilon_e^p)^{n-1} \text{ and } \sigma_e^{n-1} < \sigma_e^{n} \end{cases} \qquad (4.2)$$

Both plastic straining and strain hardening will occur if the plastic effective stress value exceeds the initial Von-Mises yield criteria, and if each increment of this stress remains greater than the previous increment. Therefore, the above expression of the flow law traces the expanding yield surface with time.

Next, a plastic strain increment is calculated based on a given time increment

$$\left\{d\epsilon_{ij}^{p}\right\}^{n} = \left\{\dot{\epsilon}_{ij}^{p}\right\} dt^{n} \qquad (4.3)$$

Furthermore, this plastic strain increment is summed with the previous increment to find the current effective plastic strain which is then used to determine the current value of $\bar{\sigma}(\epsilon_e^p)$ by

$$\bar{\sigma}(\epsilon_e^p) = \bar{\sigma}_o + H' \epsilon_e^p \qquad (4.4)$$

Figure 12 shows multilinear curves developed for each variation of the Malvern model. The top curve was the original curve developed by Hinnerichs for the linear Malvern model. The bottom two curves were developed to best fit IN-100's experimental tensile response data presented in a technical report by Stouffer (6).

UNIAXIAL RESPONSE USING A FINITE ELEMENT MODEL

The uniaxial nonlinear response of IN-100 was checked using the finite element model as shown in Figure 13

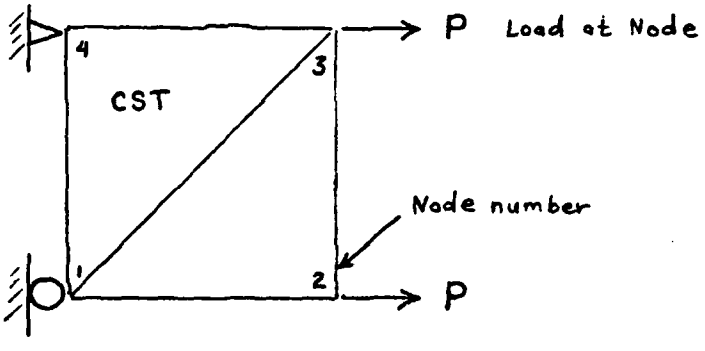

CST Elements

FIGURE 13. FINITE ELEMENT MODEL USED FOR UNIAXIAL RESPONSE

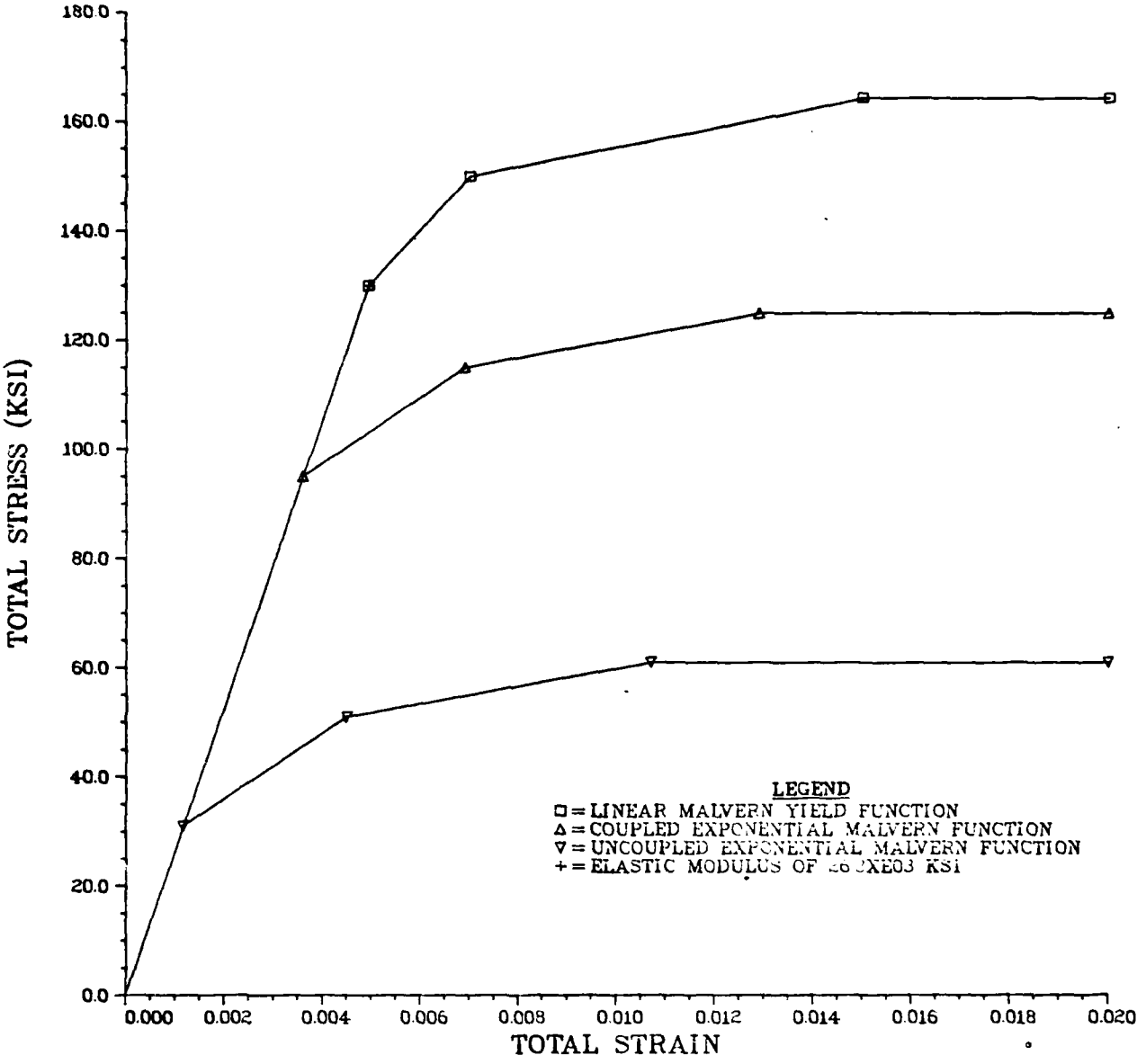

FIGURE 12. STRAIN HARDENING YIELD FUNCTIONS USED IN VARIOUS VERSIONS OF THE MALVERN OVERSTRESS FLOW LAW.

These elements were subjected to various load levels to determine how the nonlinear stress-strain response of the coupled Malvern-Norton compared to that of the Bodner-Partom. Figure 14 shows the nonlinear uniaxial finite element response of the Bodner-Partom flow law versus the exponential Malvern using an applied stress of 164.4 KSI. The exponential Malvern using the multilinear strain hardening yield stress function matches the Bodner stress-strain response well.

For the Malvern flow law, the curved inelastic response is highly dependent on the universal strain hardening yield stress function. This function was developed by performing a multilinear fit to actual experimental stress-strain curve data as discussed in the theory section.

THE FINITE ELEMENT METHOD APPLIED TO ELASTIC-PLASTIC STRUCTURES

In an isotropic material in which the yield point (uniaxially) has been exceeded, strain hardening will occur and, therefore, elastic analysis is invalid. When modeling elastic-plastic material with finite elements, a numerical iteration process must be used to account for the material's changing stiffness within the plastic region. Either the element's stiffness coefficients can be updated or a technique known as the residual overstress force method (18), can be used. This method uses an incremental inelastic strain from a viscoplastic flow law to generate a residual load vector. This vector is then added to the externally applied load vector (and multiplied by the inverse of the elastic stiffness matrix) to form total nodal displacements within an element.

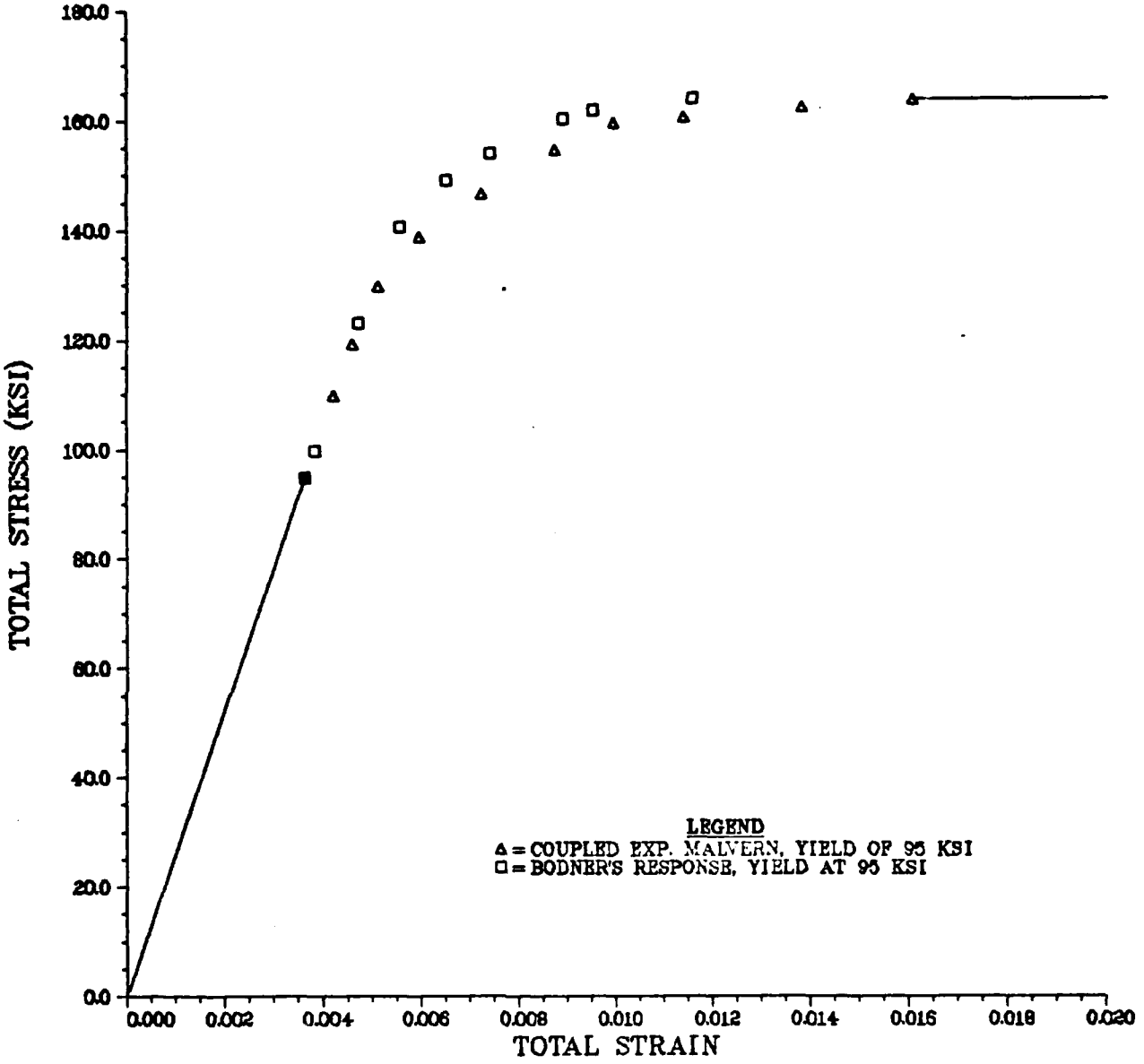

FIGURE14. COUPLED EXPONENTIAL MALVERN VERSES BODNER'S FLOW LAW USING A UNIAXIAL FINITE ELEMENT RESPONSE OF IN100 AT 1350F.

The residual load vector created by plasticity is a pseudo-force, since it is not part of the externally applied force. Thus, in computing the current stress level within an element, the plastic strain generated must be removed so that the actural stress within the structure will not exceed the externally applied stress.

The residual force method is numerically solved using the Euler integration technique in which time is incremented directly while load, strain, and stress are incremented indirectly. This method does not modify the elastic stiffness coefficients of the finite element model.

To show how this method is incremented within the computer code, the linear Malvern overstress law is used to determine a plastic strain rate and is computed as follows

$$\dot{\epsilon}_{ij}^{P} = \gamma_P \left[\frac{\sigma_e}{\bar{\sigma}(\epsilon_e^P)} - 1 \right] \frac{3}{2} \frac{S_{ij}}{\sigma_e} \tag{4.5}$$

Next, the current simulation time is determined

$$t^i = t^{i-1} + dt^i \tag{4.6}$$

Taking the element's plastic strain rate and multiplying by the time increment, the element's plastic strain increment is

$$\left\{ d\epsilon_{ij}^{P} \right\}^i = \left\{ \dot{\epsilon}_{ij}^{P} \right\} dt^i \tag{4.7}$$

then

$$\left\{ d\epsilon_e^P \right\}^i = \sqrt{\frac{2}{3} d\epsilon_{ij}^P d\epsilon_{ij}^P} \tag{4.8}$$

and

$$\{\epsilon_e^p\}^i = \{\epsilon_e^p\}^{i-1} + \{d\epsilon_e^p\}^i \tag{4.9}$$

Thus, the current effective plastic strain can then be used to determine a new value for the strain hardening yield stress function. The previous plastic strain is summed with the current plastic increment to obtain the total plastic strain

$$\{\epsilon_{ij}^p\} = \{\epsilon_{ij}^p\}^{i-1} + \{d\epsilon_{ij}^p\}^i \tag{4.10}$$

The plastic load vector (residual load vector) can be calculated

$$\{Q\}^{i-1} = \int_{VOL} [B]^T [D] \{\epsilon_{ij}^p\}^i d\,VOL \tag{4.11}$$

The current externally applied load vector is calculated

$$\{P\}^i = \{\dot{P}\}^i dt^i + \{P\}^{i-1} \tag{4.12}$$

Now, using the elastic stiffness matrix, the nodal displacements of the element are

$$\{U\}^i = [K]^{-1} \left(\{P\}^i + \{Q\}^{i-1} \right) \tag{4.13}$$

The total current strain value can be expressed by

$$\{\epsilon_{ij}\}^i = [B]\{u\}^i \tag{4.14}$$

Finally, the current total stress value within the element is expressed by,

$$\{\sigma_{ij}\}^i = [D]\left(\{\epsilon_{ij}\}^i - \{\epsilon_{ij}^P\}^i\right) \quad (4.15)$$

Note that the plastic strain within the element is removed, since the term introduced by the pseudo-force would generate a combined internal stress exceeding the applied external stress. This method is repeated for every element and the interaction process continues until the point at which stress and strain within the element satisfies equilibrium with the externally applied loads.

The uniaxial initial strain iteration scheme is graphically displayed in Figure 15.

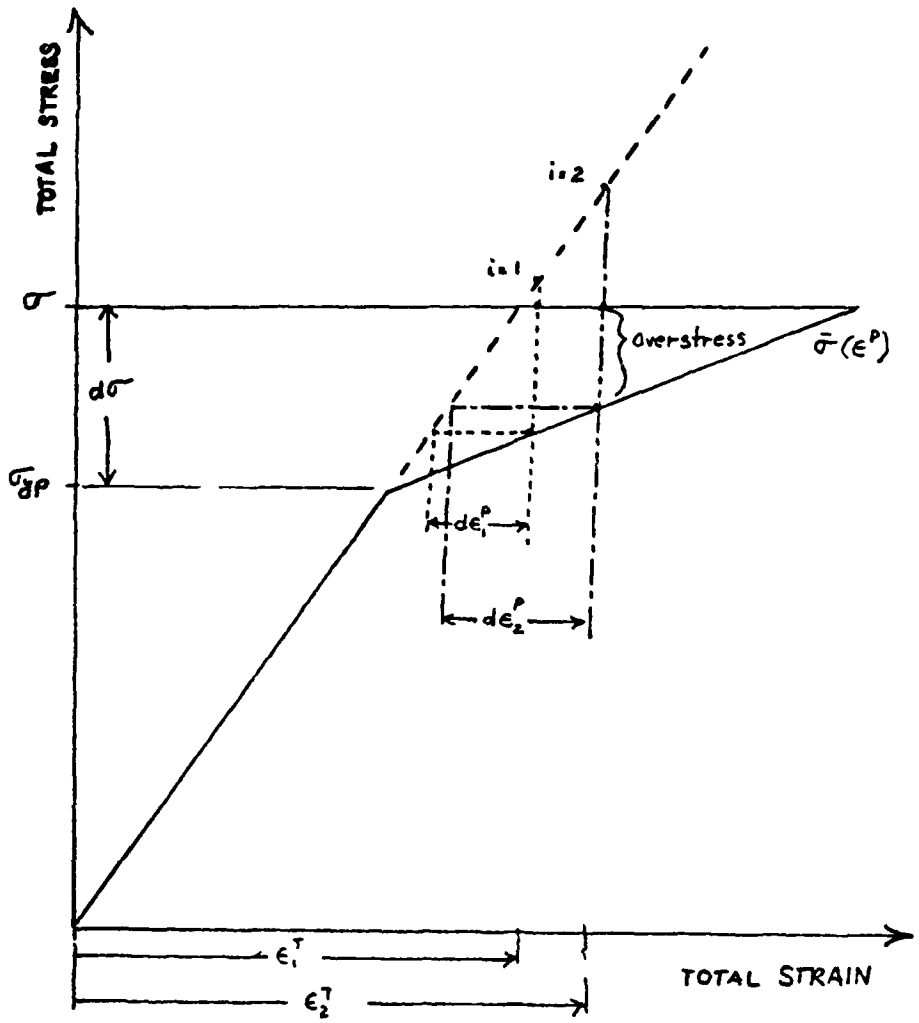

FIGURE 15. UNIAXIAL INITIAL STRAIN INTERATION SCHEME.

V. HYBRID EXPERIMENTAL NUMERICAL PROCEDURE AND THE FINITE ELEMENT MODEL

To predict crack growth within the finite element model, a method known as the Hybrid Experimental Numerical procedure is used (18). This method compares experimental crack opening displacements with nodal displacements generated by the finite element program containing one of the rate-sensitive flow laws. For example, the finite element model is loaded with an applied stress level. If the stress field intensity is high enough at the crack tip, then one of the rate sensitive models will generate plastic straining within a plastic zone region. The inelastic straining will generate near field displacements which are measured with time and compared with the experimental. Thus, if the finite element's nodal displacement rate is greater than the experimental, the node at the crack tip will remain restrained (thus, plasticity retards crack growth). Conversely, if the nodal displacement rate is less than the experimental, the node at the crack tip will be released to insure compatibility with the experimental crack opening displacement rate. A detailed discussion of how the nodal release method is employed in the program is reported by Hinnerichs (5). The experimental crack opening displacement curves have been reported by Sharpe (8) and shown in Figures 16 and 17. Thus, the Hybrid Experimental Numerical (HEN) procedure will trace experimental displacement rates rather than crack growth rates. This displacement rate method is ideally suited for crack growth studies where the amount of crack growth is very small and, therefore, becomes almost impossible to measure experimentally (380 microns/.01484 inches).

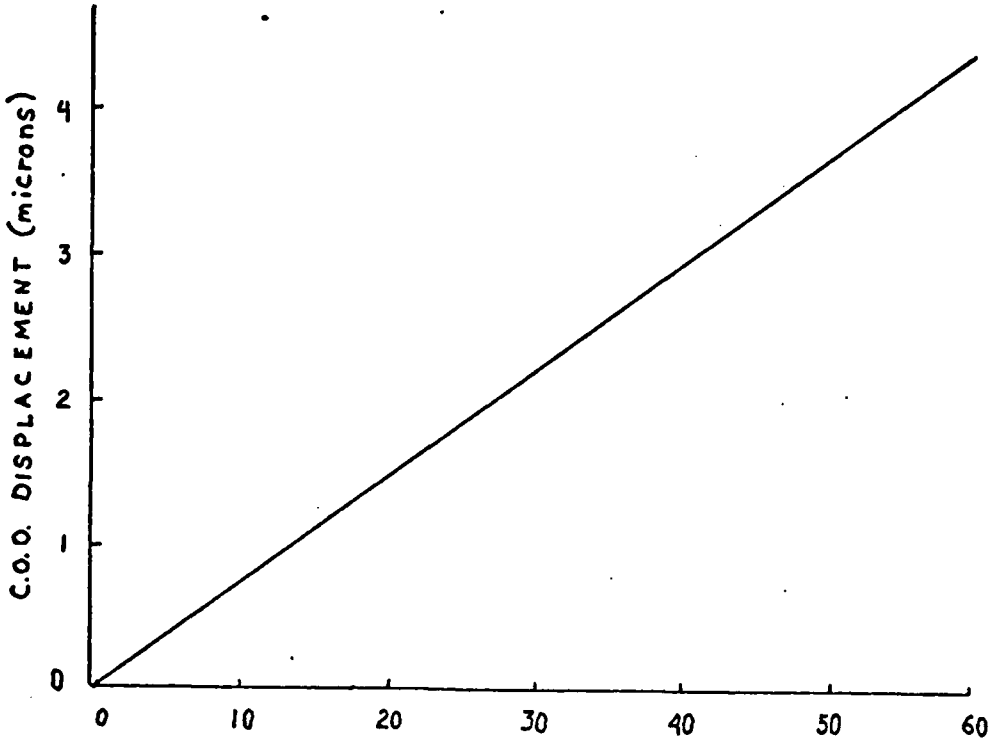

FIGURE 16. TEST 5 EXPERIMENTAL RESULTS

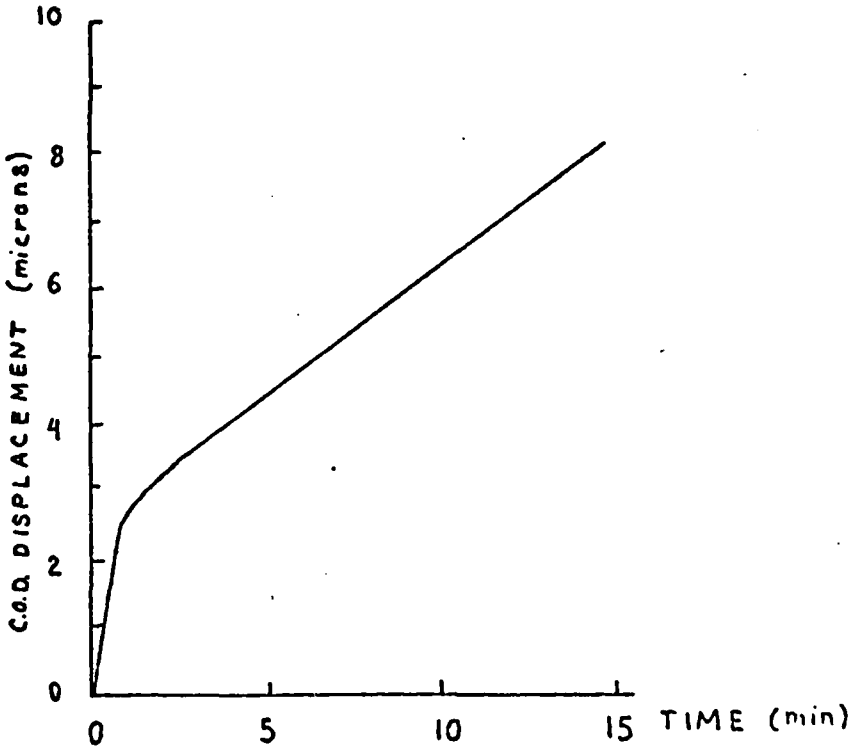

FIGURE 17. TEST 9 EXPERIMENTAL RESULTS (Sharpe, Ref. 8)

SPECIMEN MODEL FOR CRACK GROWTH. The material specimen used in the experimental tests is displayed in Figure 18. Due to this specimen's symmetry, only one quarter of the center crack plate was modeled. The finite element mesh used in modeling the test specimen is shown in Figure 19. This model consists of 355 constant strain triangles with 211 nodal points.

Convergence studies, conducted by Hinnerichs, compared model compliance with an empirical solution by Eftis and Liebowitz (20). Results indicated that the mesh had excellent convergence qualities and, therefore, the same mesh and element scheme is used in this research.

The element reduction scheme consisted of reducing element size in half until IN-100's material grain size is reached (grain size approximately 7.8125×10^{-4} inches). Figure 20 shows the refined grain size elements near the crack tip. This uniform mesh was used to insure uniform stress-strain variations as the crack grows through the material. Furthermore, grain sized elements were chosen since elastic finite element convergence studies have shown that as the rate of crack tip element size decreases, accuracy increases. Hence, a majority of the elements (218) within the finite element model can be seen in this near field crack tip region. It may be argued, from the micromechanic's point of view, that as one approaches the grain size of the material, the element's behavior can no longer be considered isotropic. But, since the finite elements are an extention of the continuum, then one can justify the use of these small elements. The number of elements used in front of the crack tip was based upon expected experimental crack growth.

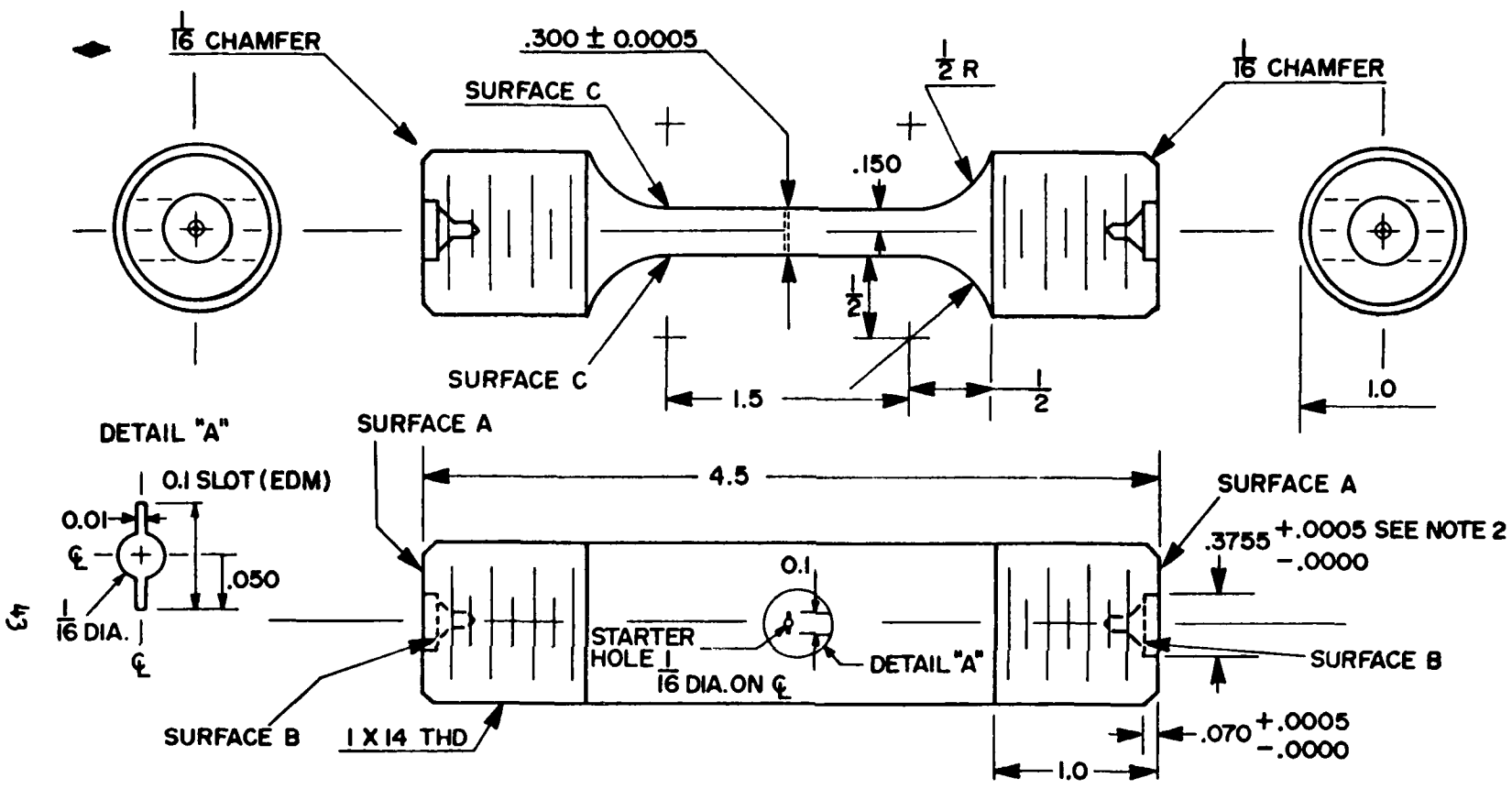

NOTES:

1. All dimensions are in inches.
2. Surfaces A and surfaces B to be parallel to within 0.0005-in.
3. Threads and 0.3755-in. holes to be concentric to within 0.001-in.
4. Threads to be concentric with each other and 0.3755 holes to be concent ic with each other to within 0.001-in.
5. Surfaces C to be square with surfaces A and surfaces B to within 0.001-in.
6. Rad. and gage section to blend smoothly without undercut.

Figure 18. Experimental Creep Crack Growth Specimen

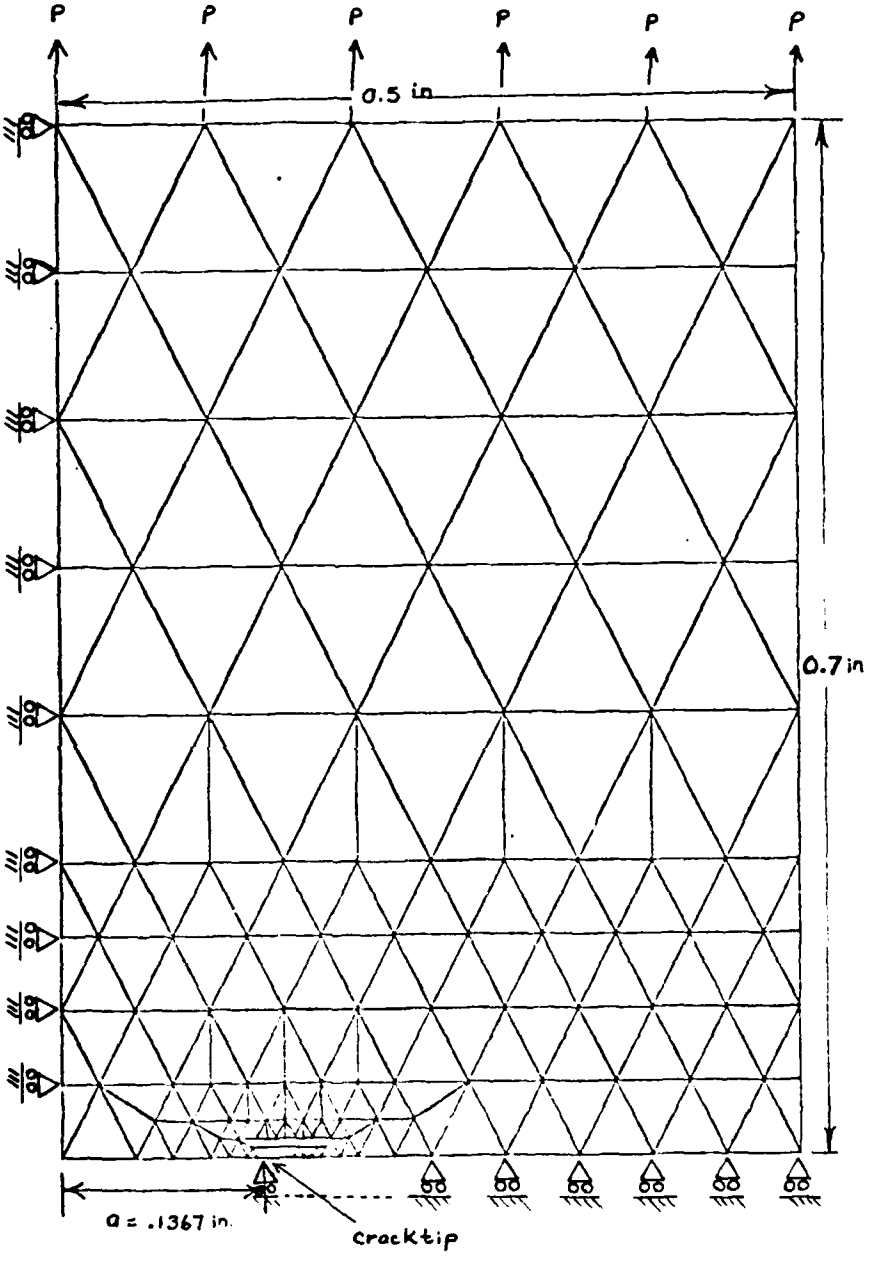

Figure 19 Center Cracked Plate Finite Element Model Showing Crack lenght and Cracktip Location.

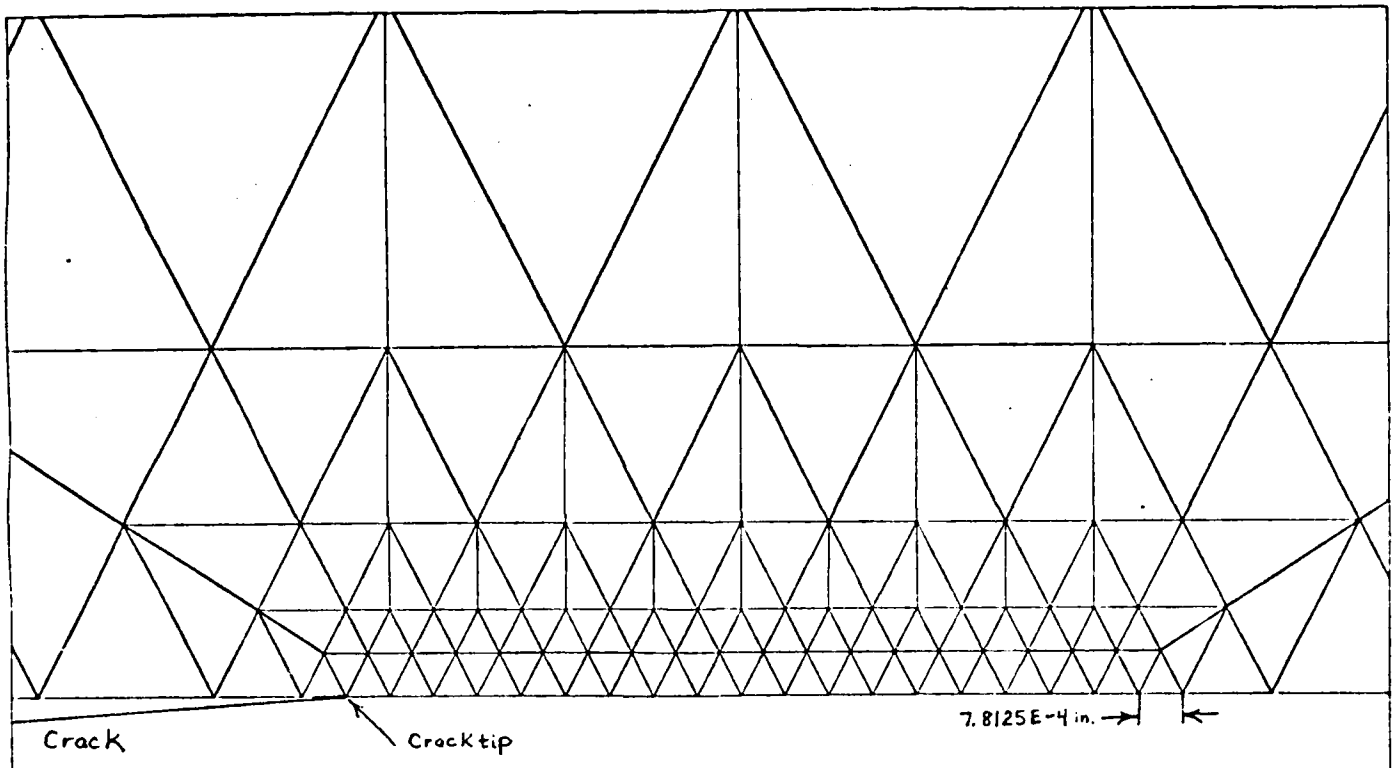

Figure 20 . Uniform Finite Element Template Showing Grain Size Elements in Front of Crack Tip.

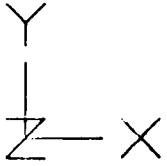

VI. RESULTS AND DISCUSSION

In comparing variations of material models, (Malvern's and Bodner's flow laws) differences in constitutive development must be kept in mind. Bodner's response is independent of an initial yield point and thus, plastic flow is initiated from the beginning of load application. On the other hand, Malvern's flow law is based on the Von-Mises yield surface and thus, plasticity does not start until the material's elastic response exceeds this surface. The computer code required that an initial yield point be specified to start plastic action with the Bodner model. Therefore, variations of the initial yield point were tried to note the effect upon Bodner's response. Using a high K value and yields of 45 KSI and 130 KSI respectively, the Bodner model shows very little change in total plastic work between the two initial yield values (see Figure 21). With such a minimal change, it was considered valid to use a starting point of 130 KSI for plastic flow. This value is used in all calculated responses of the Bodner model unless otherwise stated.

In all the comparisons made in this section, a center crack plate is used with an initial crack length of .1367 inches. The total load of the plate was applied within 5 seconds; this was the same procedure used in the experimental testing.

Different plastic zone sizes were produced by loading the finite element model to different force levels. Table 5.1 exhibits two different cases that were run using the various strain-rate sensitive models to predict plastic flow during crack growth.

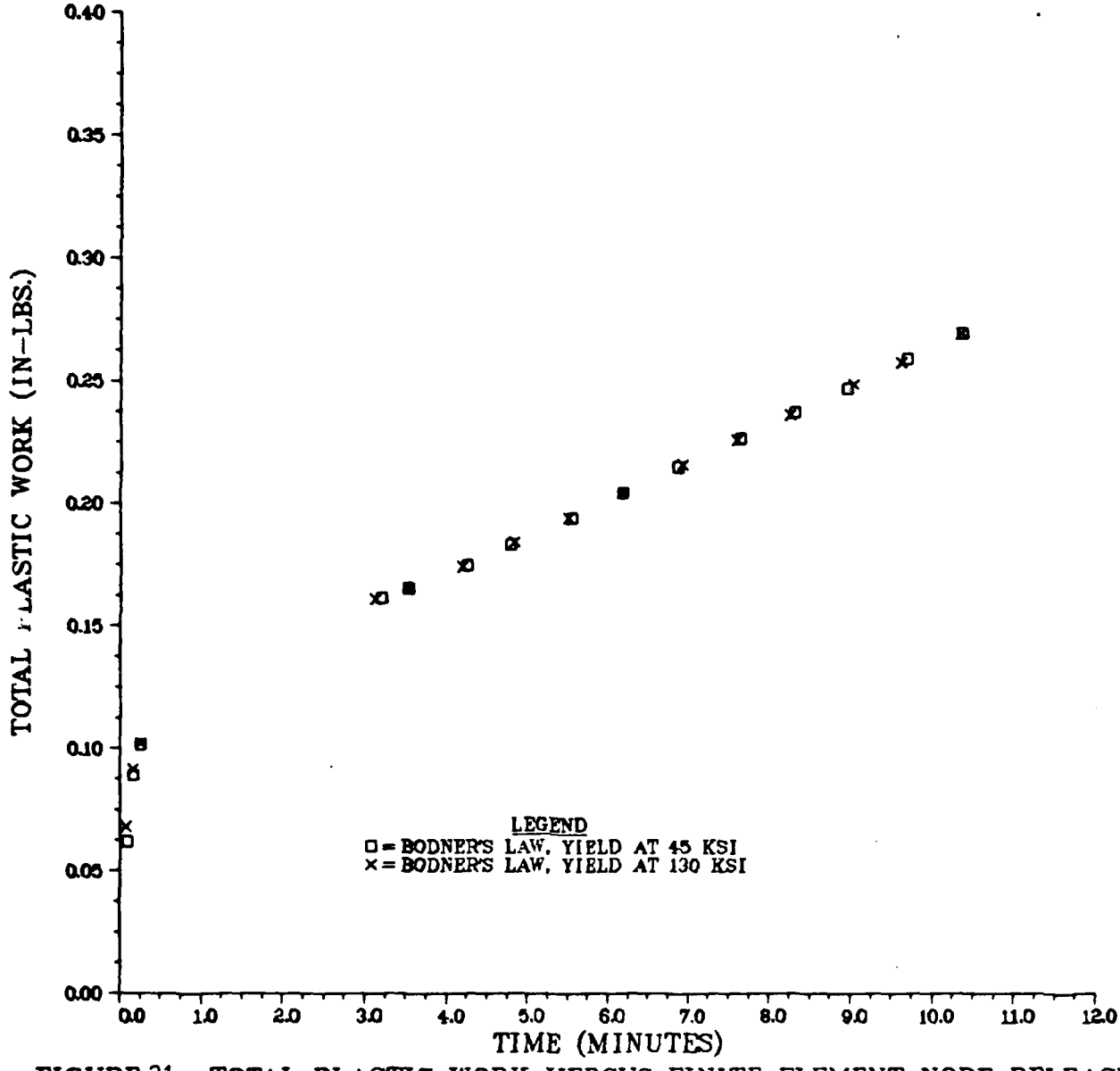

FIGURE 21. TOTAL PLASTIC WORK VERSUS FINITE ELEMENT NODE RELEASE TIMES FOR AN APPLIED LOAD OF 16060 IBS.

TABLE 5.1

EXPERIMENTAL TEST SPECIMEN CASES

Test Number	Initial Crack Length (in.)	Load (lbs.)	K_{FE} (KSI $\sqrt{in}$)	C.O.D. Indent Location From Line of Symmetry
5	.1367	10896	25.0	.1125
9	.1367	16060	36.8	.05

COMPARISONS USING TOTAL PLASTIC WORK

The total plastic work within the plastic zone is computed by (where i is the iteration increment and N is the number of finite elements)

$$W_p^i = \sum_1^N \{S_{ij}\}^i \{\dot{\epsilon}_{ij}^p\}^i dt^i \,(\text{VOL. OF ELEMENT}) \qquad (5.1)$$

where S_{ij} is the deviatoric stress vector, $\dot{\epsilon}_{ij}^p$ is the plastic strain rate determined by one of the rate-sensitive flow laws and dt is the current increment in time. This work is summed up for each element in the plastic zone which yields the total plastic work performed during inelastic deformation. As crack propagation occurs, elements behind the crack tip no longer accumulate plastic work because their stress levels are being reduced below that which causes permanent deformation. Thus, the total plastic work accumulated is a measure of the amount of plastic flow produced by the rate-sensitive models.

MODEL COMPARISONS AT LOW K LEVEL. The first comparison is made using the linear version of the Malvern flow law (K of 25 KSI $\sqrt{\text{in}}$)

$$\dot{\epsilon}_{ij}^p = \gamma_p \left[\frac{\sigma_e}{\bar{\sigma}(\epsilon_e^p)} - 1 \right] \frac{3}{2} \frac{S_{ij}}{\sigma_e} \qquad (5.2)$$

This model's strain-rate sensitivity was set using $\gamma_p = .33\ \text{sec}^{-1}$, which matches a high strain rate value of $.833 \times 10^{-2}\ \text{sec}^{-1}$, to insure this problem dependent model would predict the average strain rate occurring within the plastic zone (the $\bar{\sigma}(\epsilon_e^p)$ with its initial yield stress of 130 KSI has been previously discussed). The standard load rate is applied

to the finite element model and strain-rate sensitive model is allowed to generate plastic flow, retarding crack growth.

Figure 22 shows the linear Malvern response during crack growth. During the first 30 minutes of crack propagation, this model generates slightly more plastic work than Bodner's. This indicates that for higher stress levels, the Malvern model is more rate sensitive (i.e. $\dot{\epsilon}$ versus stress). After approximately 30 minutes of crack growth, the differences in accumulated plastic work between these models become negligible.

The next comparison is made with the material dependent coupled Malvern-Norton exponential flow law. This model's initial yield stress value was set at 95 KSI, while its γ_ρ and α values are the material's constants, as determined previously. Figure 22 shows that this model captures slightly more plastic work than either the linear Malvern or Bodner flow laws. This is due to the lower yield stress value, where a larger number of elements may produce plastic straining and generate more plastic work.

In summary, the total plastic work accumulated among all three plastic flow models is almost identical throughout the entire range of computer simulation time. This occurs since the variations (strain rate and stress) within the plastic zone are so small that each material's response to these variations becomes insignificant. It can also be noted from Figure 22 that the rate of total plastic work accumulated is constant (i.e. slope of W_p versus time).

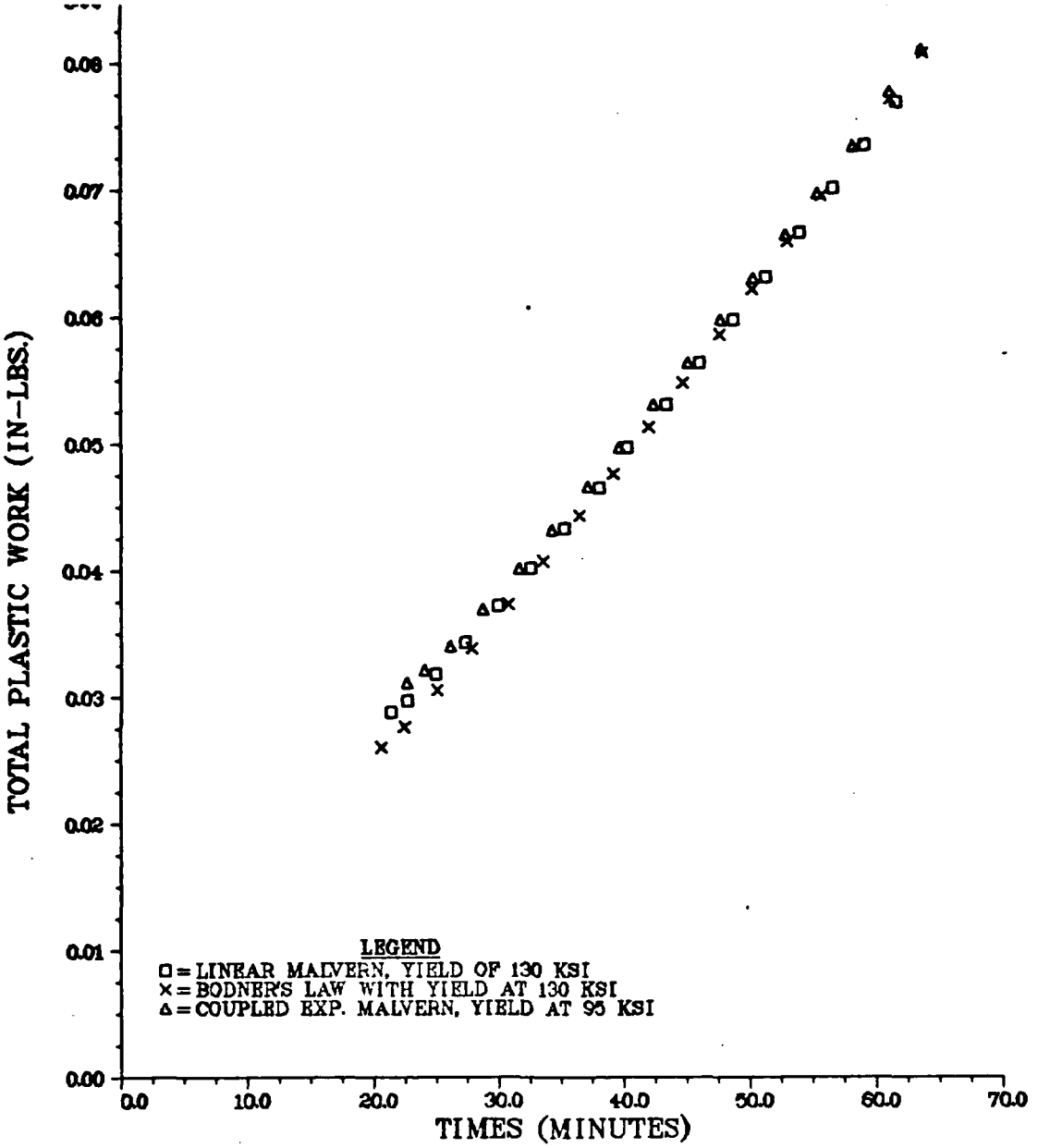

FIGURE 22. TOTAL PLASTIC WORK VERSES FINITE ELEMENT NODE RELEASE TIMES FOR AN APPLIED LOAD OF 10869 LBS.

MODEL COMPARISONS AT HIGH K LEVEL. The next test involved an applied load of 16060 lbs., producing a K value of 36.8 KSI in . The magnitude of the effective stress within the finite elements near the crack tip immediately after total stress application ranged from 160 to 170 KSI. Thus, the plastic zone size is larger than in the low K test, with a greater variation of plastic strain rates and stress in this zone. Figure 23 shows that the coupled exponential Malvern-Norton model accumulates more plastic work than either the linear Malvern or Bodner models. This is based on the fact that this model was formulated with an initial yield stress value of 95 KSI, (see theory section for discussion) generating plastic flow when this stress value is exceeded. On the other hand, the problem dependent linear Malvern matches only one experimental strain rate (i.e. $.833 \times 10^{-2}$ sec^{-1}) and is set with an initial yield of 130 KSI. Hence, the linear Malvern cannot accumulate the same amount of plastic work as the exponential form, but its averaging technique shows good correlation with the Bodner-Partom model.

Figure 24 shows the response of the uncoupled exponential Malvern (Norton is not included) versus the Bodner-Partom. In this case, the initial yield stress for both models is set at 45 KSI. The uncoupled exponential Malvern continues to accumulate more plastic work than the Bodner-Partom. This indicates that the Malvern model, in exponential form, is more rate-sensitive (slope of predicted $\dot{\epsilon}$ versus stress curve) to stress variations than either the Bodner or linear Malvern.

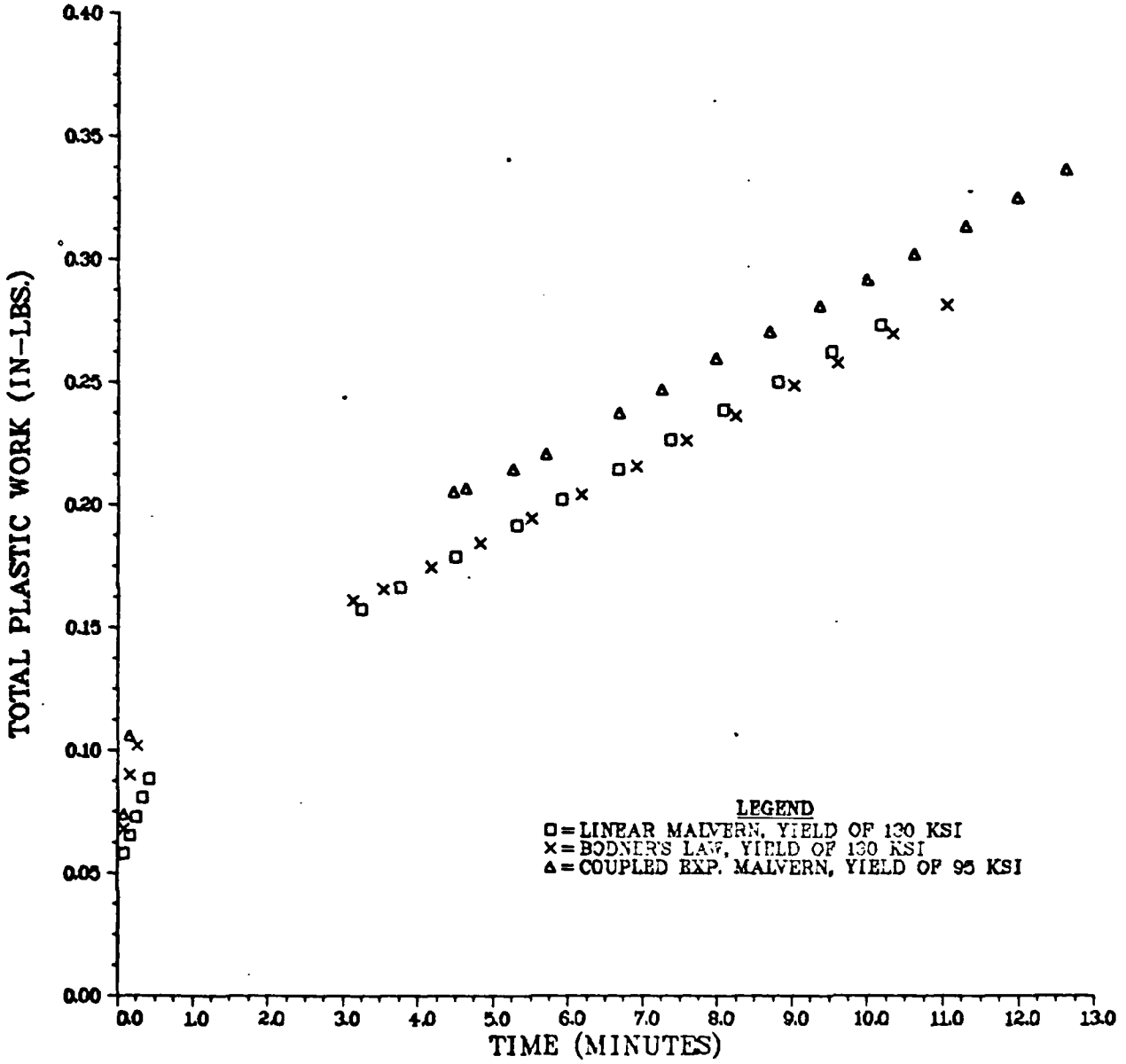

FIGURE23.TOTAL PLASTIC WORK VERSES FINITE ELEMENT NODE RELEASE TIMES FOR AN APPLIED LOAD OF 16060 LBS.

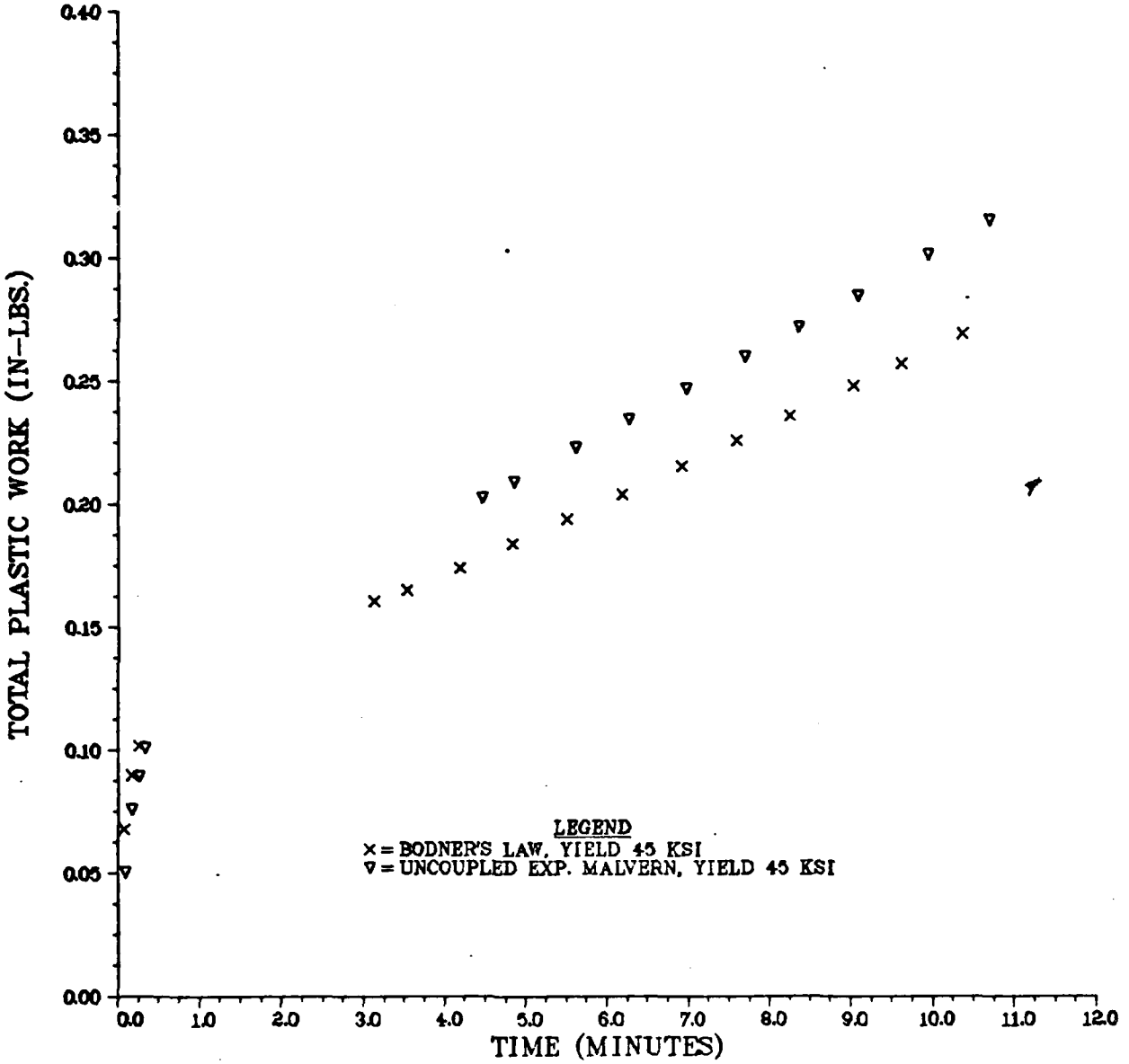

FIGURE 24 TOTAL PLASTIC WORK VERSUS FINITE ELEMENT NODE RELEASE TIMES FOR AN APPLIED LOAD OF 16060 LBS.

CRACK LENGTH AND RATE COMPARISONS. During the finite element simulation runs, load is applied within 5 seconds, but no crack growth is allowed. Hence, in the vicinity of the crack tip, a large stress field develops in which a rate-sensitive model initiates plastic flow. The amount of plastic flow generated is highly dependent on the model's plastic strain sensitivity at various load levels. These sensitivities (slope of the $\dot{\epsilon}$ versus stress curve) and each model's ability to capture ranges of plastic strain variations effect the crack growth behavior of each model.

Results shown in Figure 25 for the low K value, indicate that all three models are predicting approximately the same crack growth rate and final crack length. This is due to the small plastic zone size where variations in stress and strain rates are small, thus, the viscoplastic flow captured by each model is almost insignificant.

Figure 26 depicts the model variations when the high K level is used with the same initial crack length. The differences in each model's rate-sensitivity become apparent, since the plastic zone size and variations in plastic strain rate and stress are much larger. The problem dependent linear Malvern model exhibits the greatest amount of crack growth per unit of time. This result indicates that the problem dependent model, which predicts only one strain rate accurately, is not capturing as much plastic strain as either the Bodner or coupled exponential Malvern model.

The coupled exponential Malvern-Norton model shows the least amount of crack growth per unit time when compared to the other flow law models.

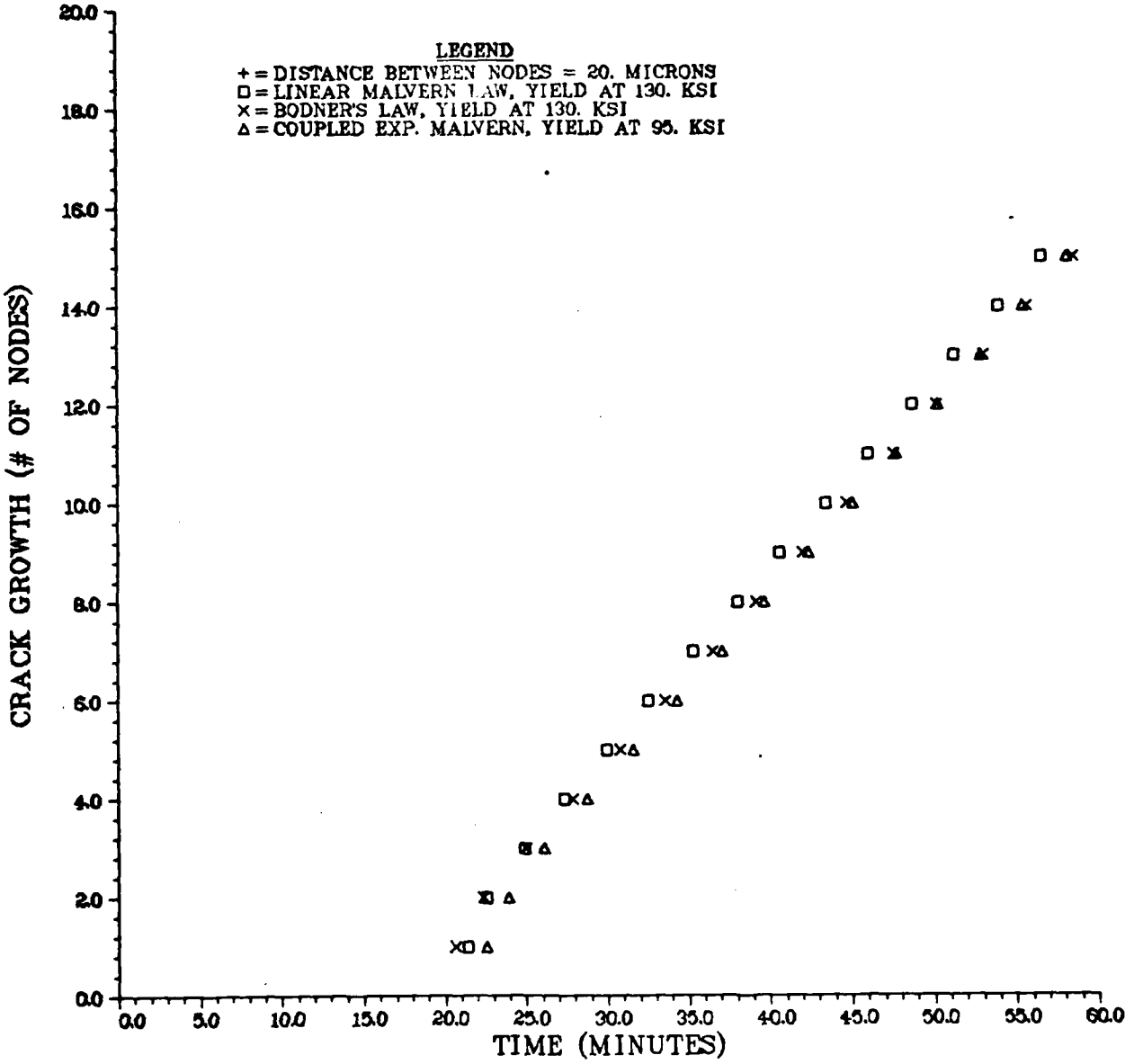

FIGURE 25. NUMBER OF NODES RELEASED VERSUS TIME FOR VARIOUS FLOW LAWS WITH AN APPLIED LOAD OF 10896 LBS.

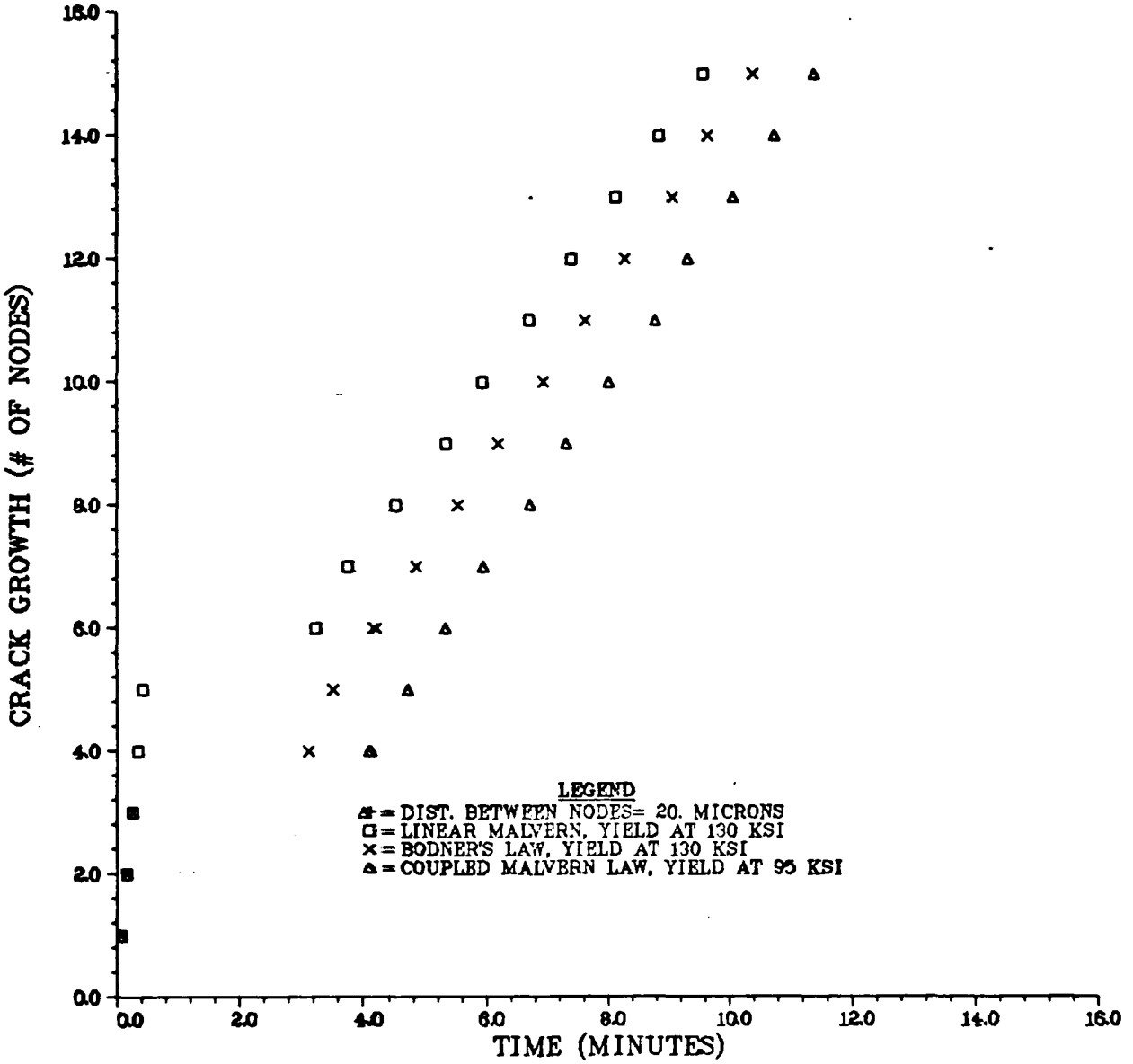

FIGURE 26. NUMBER OF NODES RELEASED VERSUS TIME FOR VARIOUS FLOW LAWS WITH AN APPLIED LOAD OF 16060 LBS.

This indicates that the coupled exponential expression is generating more plastic strain near the crack tip which retards the amount of crack growth. Therefore, the exponential Malvern is more sensitive to strain rate variations for a given stress level than either the Bodner or linear Malvern. This fact becomes clear upon examination of the stress contours and profiles for the near crack tip region.

Figure 27 shows the crack growth results using the uncoupled exponential Malvern (Norton's Secondary Creep Law is not included) versus the Bodner-Partom law. The uncoupled exponential form behaves much like the coupled exponential form in predicting plastic flow near the crack tip, since the crack growth rates and final crack length are almost identical. This should be expected because both the uncoupled and coupled exponential Malvern expressions were formulated with almost identical strain rate sensitivities (i.e. slope $\dot{\epsilon}$ versus stress curve). The only difference is that the coupled exponential was matched to strain rates above 10^{-5} sec^{-1}, while the uncoupled exponential was matched to a range of strain rates above 10^{-9} sec^{-1} (this was discussed in a previous section).

A summary of the final crack lengths (a_f) predicted by the various rate-sensitive models is tabulated in Table (5.2).

COMPARISONS OF EFFECTIVE STRESS CONTOURS AND PROFILES. The effective stress contours were generated by use of an interactive graphics package MOVIE. BYU, that has been installed on the Materials Lab Prime 550 computer. The vector and scalar functions generated by Hinnerich's program were modified so that its format is compatible with MOVIE'S. This graphics package has the ability to magnify a small region so that

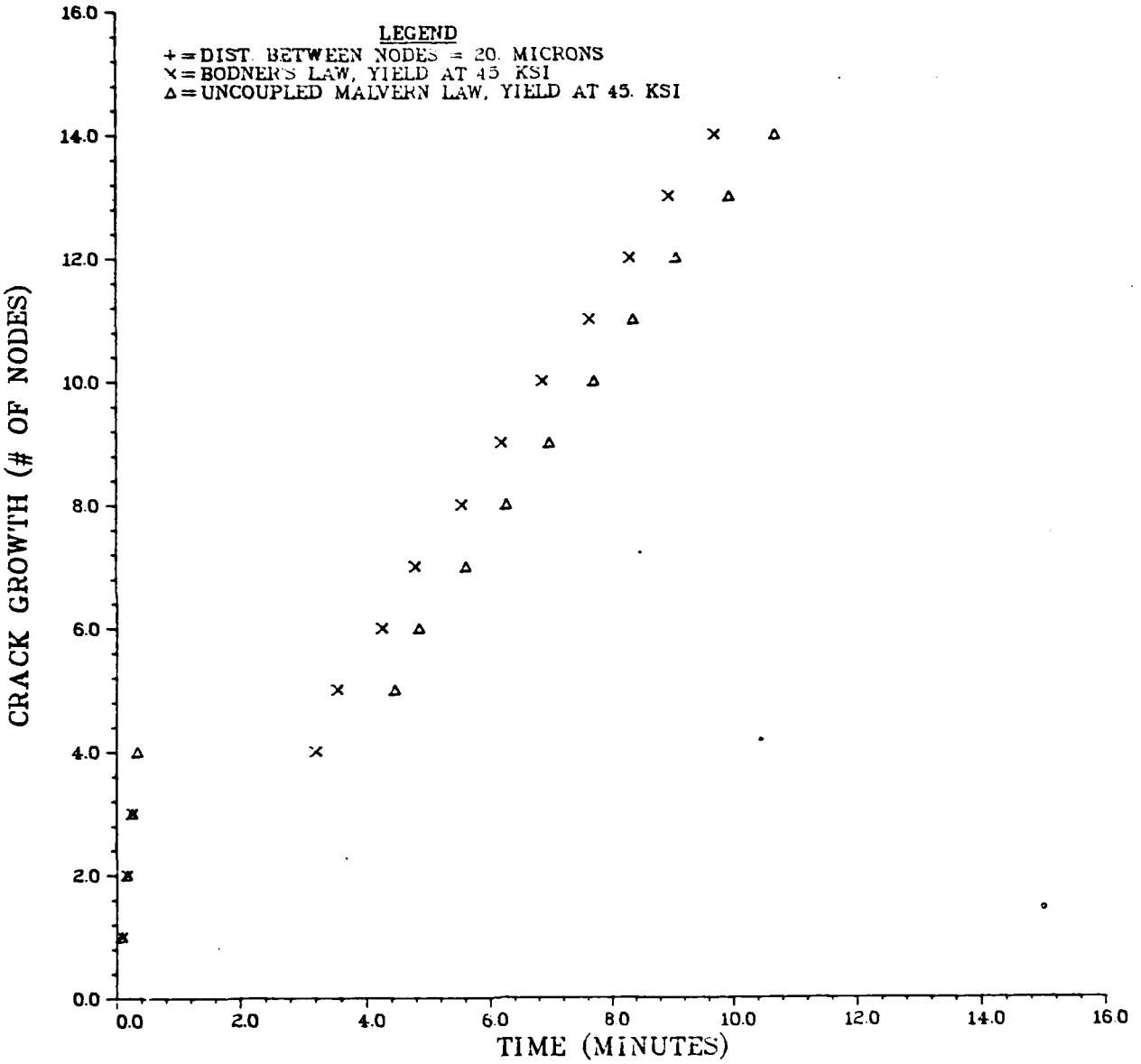

FIGURE 27. NUMBER OF NODES RELEASED VERSUS TIME FOR THE BODNER AND UNCOUPLED MALVERN FLOW LAWS WITH APPLIED LOAD OF 16060 LBS.

TABLE 5.2

SUMMARY OF CRACK GROWTH RESULTS

MODEL	LOAD (lbs.)	a_o(in.)	a_f(in.)	TIME (min.)
Linear Malvern	10896	0.1367	0.14795	55
Coupled Exp. Malvern	10896	0.1367	0.14748	55
Bodner-Partom	10896	0.1367	0.14748	55
Linear Malvern	16060	0.1367	0.14889	10
Coupled Exp. Malvern	16060	0.1367	0.14778	10
Uncoupled Exp. Malvern	16060	0.1367	0.14686	10
Bodner-Partom	16060	0.1367	0.14795	10

scalar or vector functions can be graphically displayed.

Figures 28, 29, and 30 show the effective stress contours of each rate-sensitive model generated by MOVIE immediately before the first node is released. The contours near the crack tip are very close together, indicating a sharp rise in the stress level. In comparing these contours, the contours of the coupled exponential Malvern indicate both a higher level and concentration of stress near the crack tip than either the Bodner or linear Malvern models. The linear Malvern model shows the least concentration of effective stress near the crack tip. This indicates that the linear Malvern captures the least amount of plastic strain, while the exponential Malvern captures the most plastic strain.

Figure 31 shows the effective stress levels plotted graphically versus horizontal distance from the crack tip. This plot confirms that the exponential Malvern generates a higher level of stress concentration at the crack tip, while the linear Malvern shows the least concentration.

Figures 32 and 33 exhibit the effective stress contours before the 5th node is released. Here, the magnitudes of the effective stress have been reduced from their initial load-up levels by crack propagation. When compared with Bodner's contours, the coupled exponential Malvern indicates a higher level of stress concentration near the crack tip. The exponential Malvern generates slightly more viscoplastic action (plastic strain) than Bodner's for high stress levels.

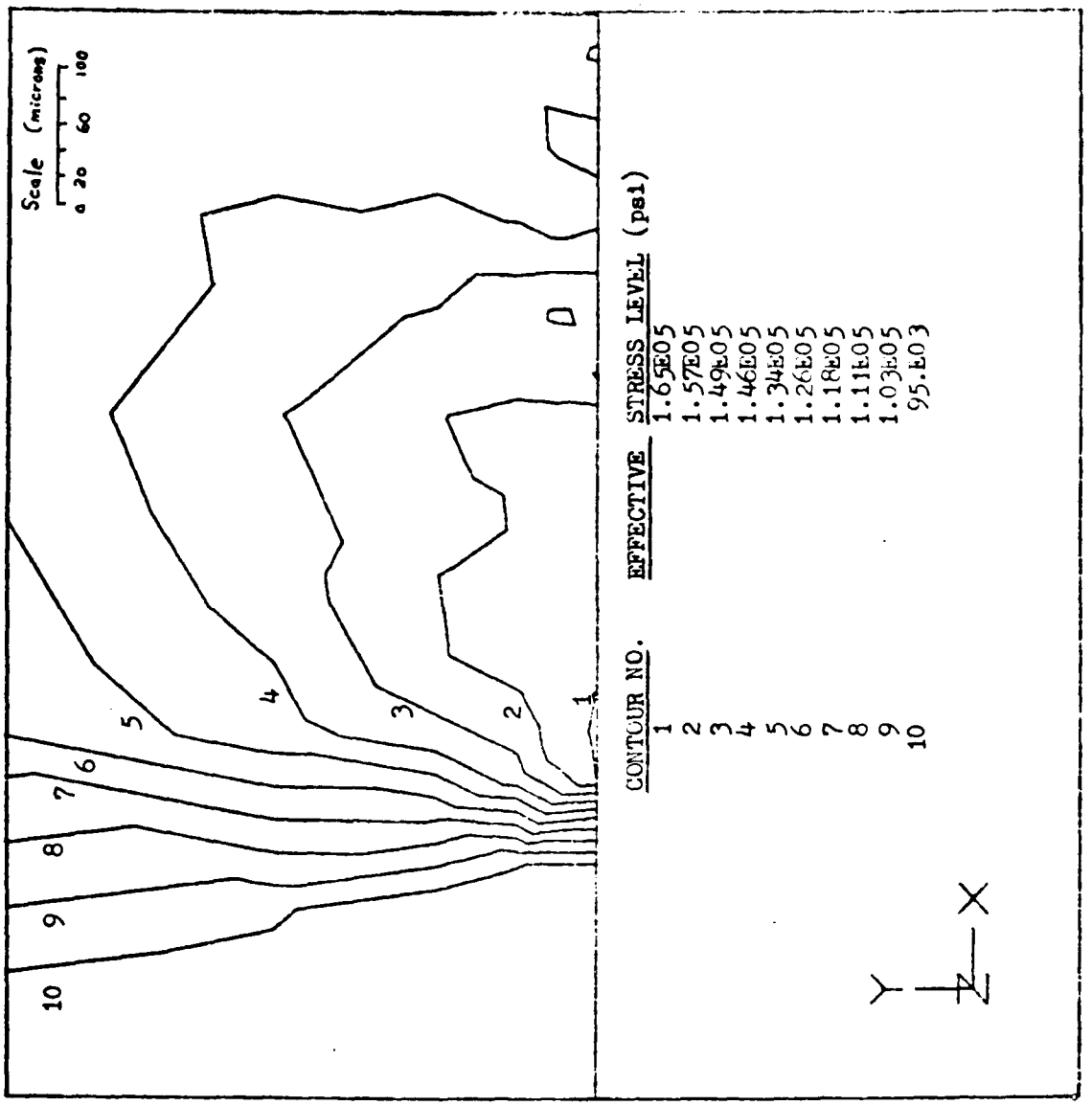

FIGURE 28 . STRESS CONTOURS NEAR CRACK TIP AT HIGH K LEVEL USING THE LINEAR MALVERN FLOW LAW.

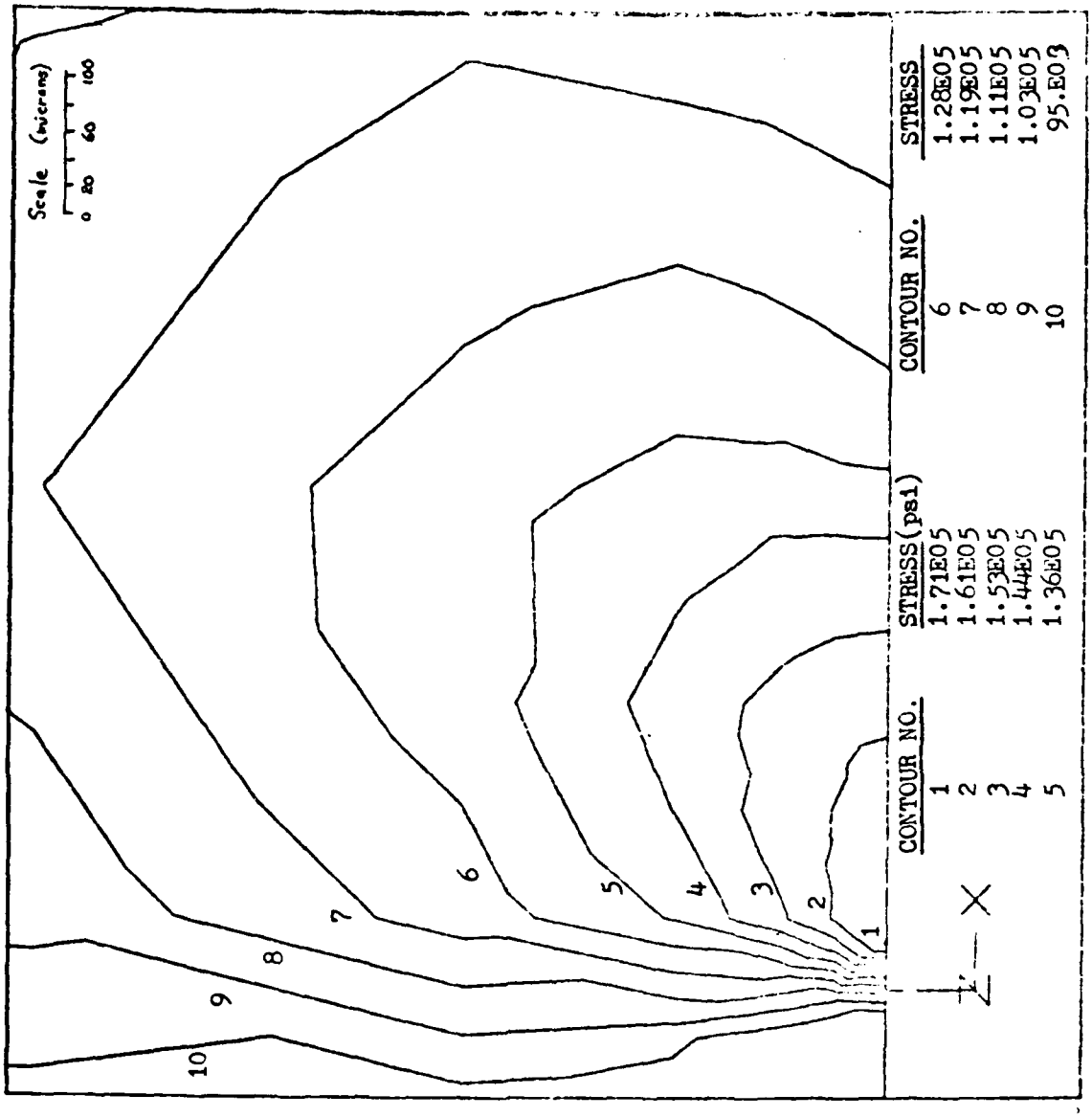

FIGURE 29. EFFECTIVE STRESS CONTOURS NEAR CRACK TIP AT HIGH K LEVEL, USING THE COUPLED EXPONENTIAL MALVERN FLOW LAW.

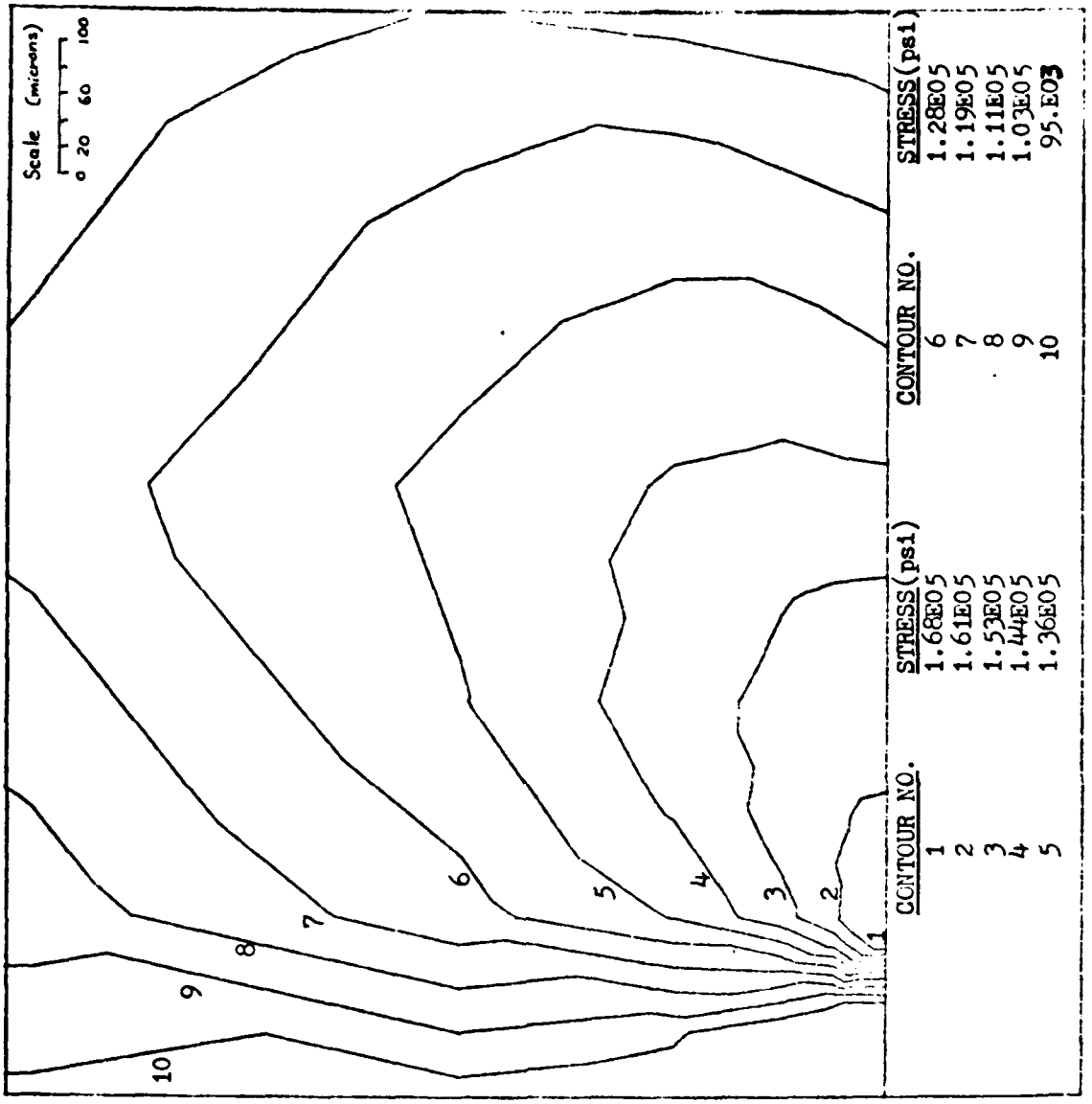

FIGURE 30. EFFECTIVE STRESS CONTOURS NEAR CRACK TIP AT HIGH K LEVEL, USING THE BODNER-PARTOM FLOW LAW.

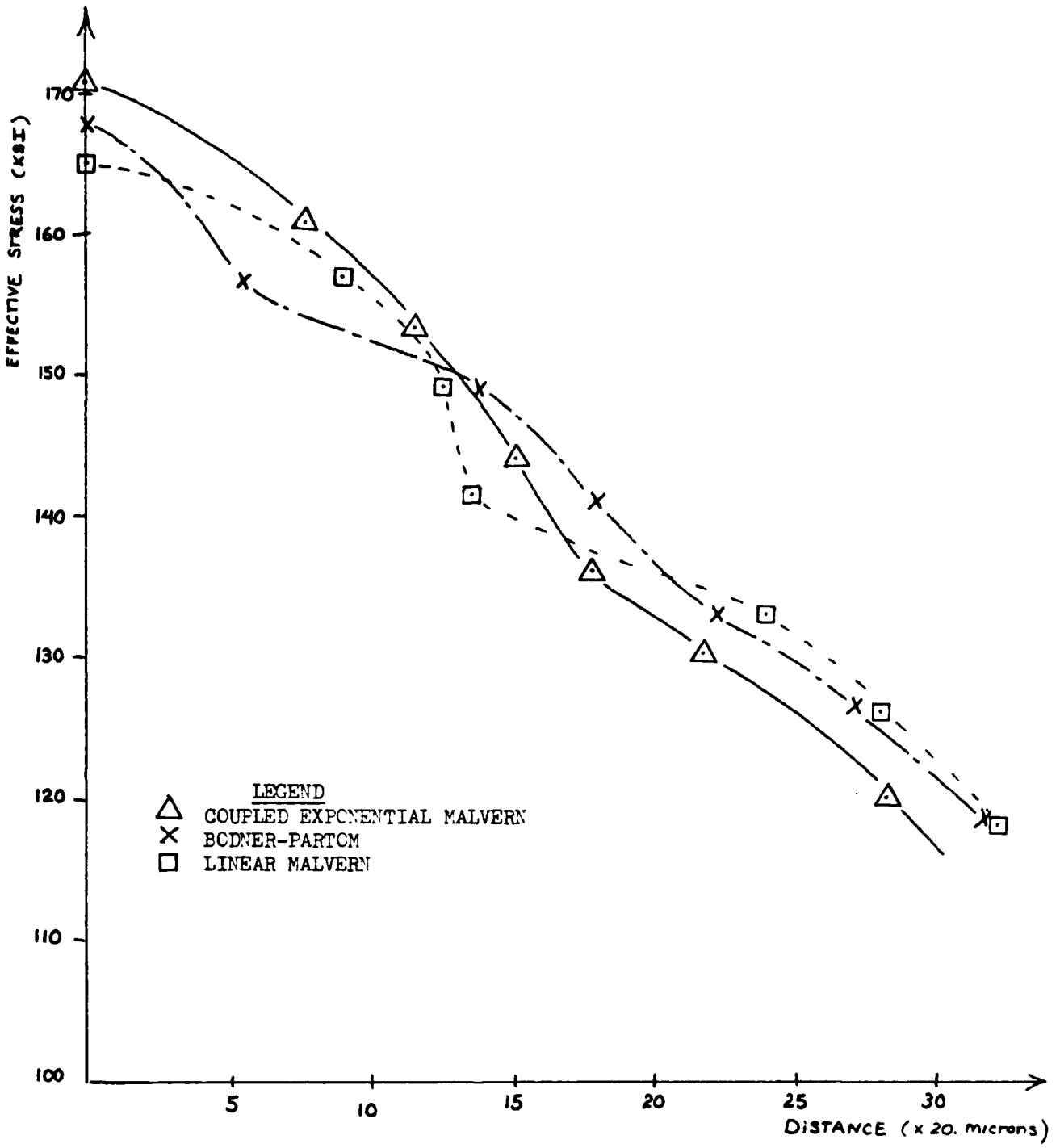

FIGURE 31. EFFECTIVE STRESS VERSUS HORIZONTAL DISTANCE MEASURED FROM CRACK TIP BEFORE 1st NODE RELEASE , AT HIGH K LEVEL.

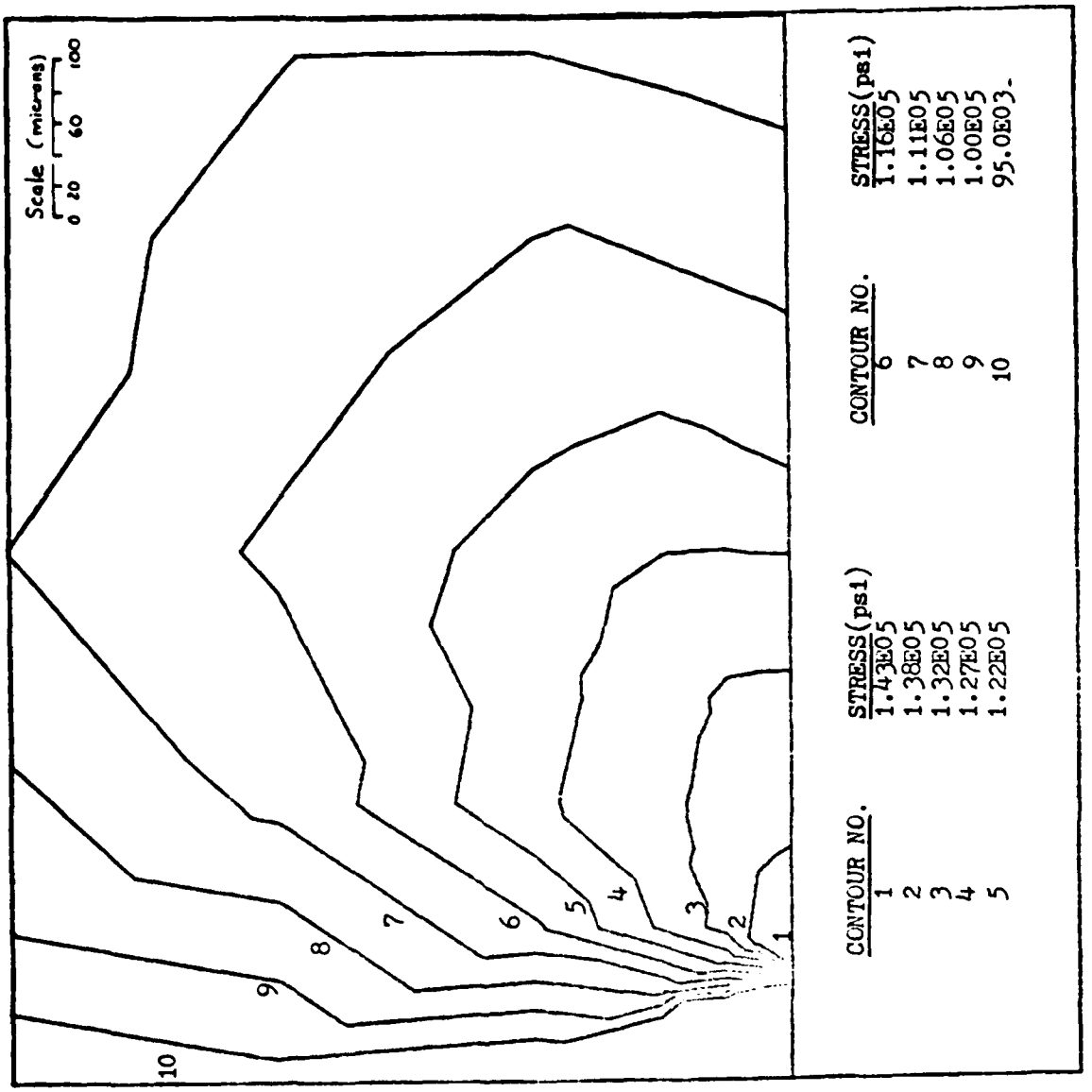

FIGURE 32 EFFECTIVE STRESS CONTOURS AFTER 4 NODES HAVE BEEN RELEASED , USING THE CCUPLED EXPONENTIAL MALVERN MODEL AT HIGH K.

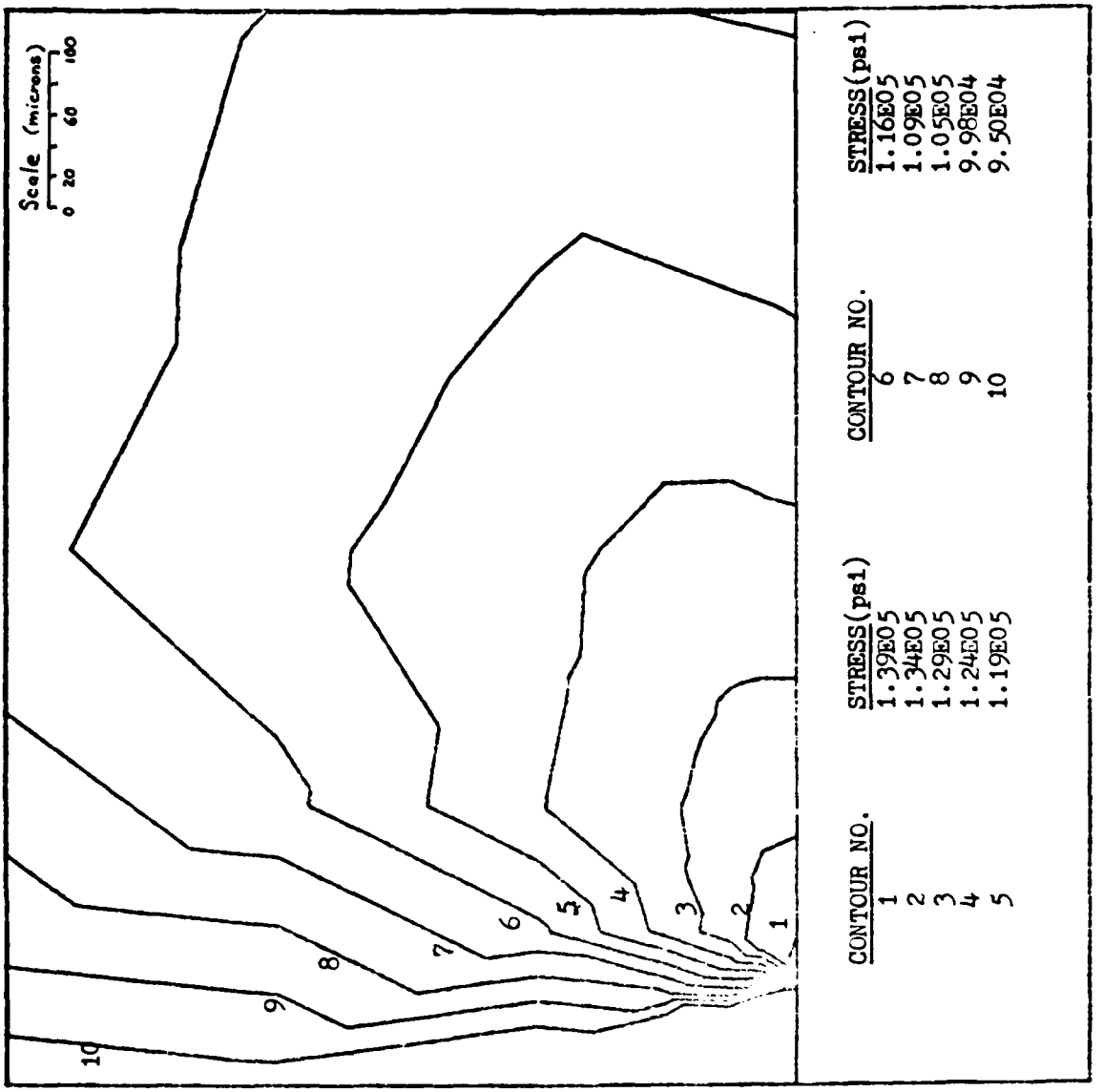

FIGURE 33. EFFECTIVE STRESS CONTOURS AFTER 4 NODES HAVE BEEN RELEASED USING THE BODNER-PARTOM MODEL AT HIGH K LEVEL.

Figure 34 represents effective stress levels plotted graphically versus horizontal distance from the crack tip. The coupled exponential shows slightly higher magnitudes of stress level near the crack tip than the Bodner, but the exponential does depict similar characteristics as the Bodner for the problem studied.

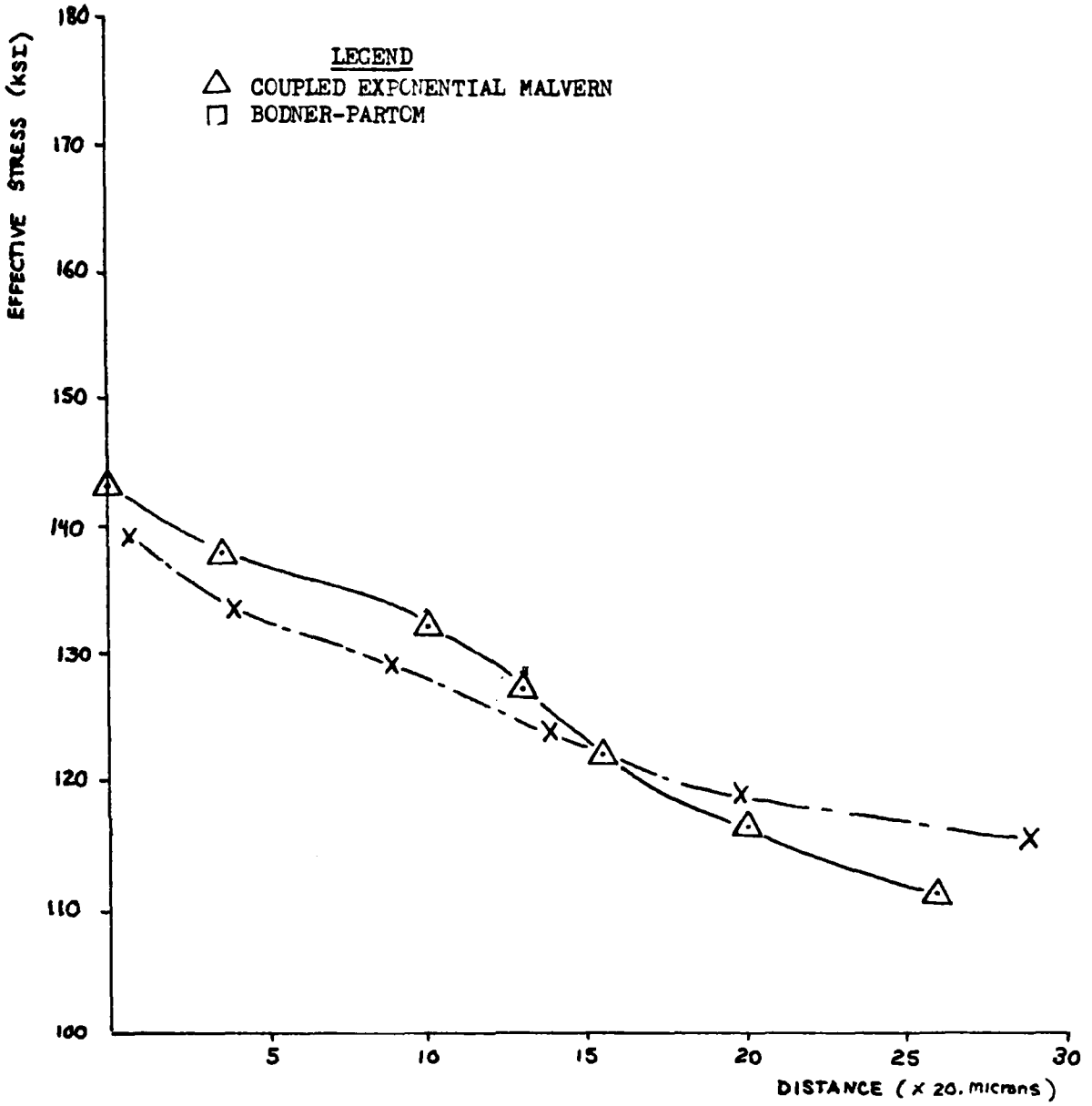

FIGURE 34. EFFECTIVE STRESS VERSUS HORIZONTAL DISTANCE MEASURED FROM CRACK TIP BEFORE 5th NODE RELEASE, AT HIGH K LEVEL.

VII. CONCLUSIONS

1. In the analysis of crack growth with various rate-sensitive models, variations in crack growth due to the response of these models are negligible when small crack lengths and stress intensities are used (less than .32% variation in final crack length between models).

However, as the stress intensity factor is increased, for the same crack length, variations in each of the model's rate sensitivity become apparent. For the high load level, the exponential forms (both coupled and uncoupled Malvern), consistently generated more plastic strain than the other flow laws. This effect was noticed by observing plastic work, effective stress, and the final crack lengths. On the other hand, variations in crack growth caused by these differences were less than one percent when comparing each model's crack lengths.

2. The linear Malvern flow law was found to be highly problem dependent. Thus, it is not practical for use in problems where either the stress level or strain rate is unknown.

3. The Bodner-Partom constitutive model should be used as a standard for other model comparisons, since this model's response is independent of the material's yield stress. Previous crack growth predictions using the Bodner model (research at AFIT by Terry Hinnerichs) demonstrated that this model generates plastic action that predicts crack growth accurately. The disadvantage lies in the determination of nine material parameters.

These parameters are coupled to each other so constitutive formulation is difficult without a thorough understanding of the model's interactions.

4. Contrary to the Bodner model, the two material parameters required for the exponential Malvern flow law are easily determined from experimental strain-rate versus stress data. The exponential response compares well with the Bodner in capturing similar amounts of plastic flow.

5. The uncoupled and coupled exponential Malvern expressions proved that the yield stress value can be arbitrarily set. Thus, these models begin to resemble the response of the Bodner-Partom which is independent of a yield stress.

When using the exponential flow laws within the finite element model, the yield stress value must be set high enough to insure that at least some elements around the perimeter of the model behave elastically. If this is not insured, then the entire model will undergo plastic failure.

6. The results obtained using the exponential form of the Malvern flow law are encouraging. But, further research should be performed using larger initial crack lengths and stress intensity factors. In these cases, further experimentation needs to be performed to insure the flow law is modeling the material's response accurately at these higher levels of stress intensities.

BIBLIOGRAPHY

1. Harris, J.A., Sims, D.L., Annis, C.G. Jr., "Concept Definition: Retirement For Cause of F100 Rotor Components", AFWAL-TR-80-4118, Wright Patterson Air Force Base, 1980.

2. Cargill, J.S., Malpani, J.K., Cheng, Y.W., "Part 1: F100 1ST-STAGE TURBINE DISK (IN 100), AFML-TR-79-4173, PART 1, Wright Patterson Air Force Base, 1979.

3. Duggan T.V., "Philosophy of Safe Life Design", Tech. Report No. F 352, Portsmouth Polytechnic, Portsmouth, England, 1980.

4. Wallace, R.M., Annis, C.G. Jr., and Sims D.L., "Application of Fracture Mechanics at Elevated Temperatures", AFML-TR-76-176, Part II, Wright Patterson Air Force Base, 1977.

5. Hinnerichs, T.D., "Viscoplastic and Creep Crack Growth Analysis By the Finite Element Method". PhD Dissertation, Air Force Institute of Technology, Wright Patterson Air Force Base, 1980.

6. Stouffer, D.C., "A Constitutive Representation For IN 100", AFWAL-TR-81-4039, Wright Patterson Air Force Base, 1981.

7. Zienkiewicz, O.C. and Cormeau, I.C., "Visco-Plasticity-Plasticity and Creep In Elastic Solids- A Unified Numerical Solution Approach", International Journal for Numerical Methods In Engineering, Vol. 8, 821-845, 1974.

8. Sharpe, W.N. Jr., and Martin, D.R., "Optical Measurement of In-Plane Strain/Displacement Near Crack Tips at High Temperature", Sixth Int'l Congress on Experimental Stress Analysis, Munich, 1978.

9. Bodner, S.R. and Partom, Y., "Constitutive Equations for Elastic-Viscoplastic Strain Hardening Materials", Journal Applied Mechanics Trans. ASME, 42, 385-389, 1975.

10. Zienkiewicz, O.C. The Finite Element Method, 3rd Edition, McGraw-Hill (UK) Limited, 1977.

11. Hult, J.A.H., Creep In Engineering Structures, Blaisdell Publishing Co., Waltham, Mass., 1965.

12. Mendelson, A., "Plasticity Theory and Application", Collier-Macmillan Limited, London, England, 1968.

13. Dieter, G.E., Mechanical Metallurgy, (Secong Edition), McGraw-Hill, 1976.

14. Malvern, L.E., Introduction to the Mechanics of a Continuous Medium, Prentice-Hall, Inc., Englewood Cliffs, N.J., 1969.

15. Malvern, L.E., "The Propagation of Longitudinal Waves of Plastic Deformation in a Bar of Material Exhibiting a Strain-Rate Effect", J. Appl. Mech., 18, 203-208, 1951.

16. Nicholas, T., "On The Determination of Constitutive Equations From Plastic Wave Propagation Phenomena", AFML-TR-73-73, Wright Patterson Air Force Base, 1973.

17. Bodner, S.R., "Representation of Time Dependent Mechanical Behavior of Rene 95 by Constitutive Equations", AFML-TR-79-4116, Wright Patterson Air Force Base, 1979.

18. Armen, H., "Assumptions, Models and Computational Methods for Plasticity", Computers and Structures, Vol. 10, 161-174, 1978.

19. Donath R.C., "Crack Growth Behavior of Alloy IN 100 Under Sustained Load At 732 C (1350 F). AFWAL-TR-80-4131, Wright Patterson Air Force Base, 1981.

20. Eftis, J. and Liebowitz, H., Int'l Journ. of Fract. Mech., Vol. 8, No. 4, December, 1972.

APPENDIX A

DETERMINATION OF NORTON'S CREEP PARAMETERS

Norton's secondary creep equation in uniaxially form is

$$\dot{\epsilon}^c = \gamma_p (\sigma)^{\beta} \qquad \text{(A 1.1)}$$

which can be rewritten by taking the natural logarithm of each side

$$Ln\ \dot{\epsilon}^c = Ln\ \gamma_c + \beta\ Ln\ (\sigma) \qquad \text{(A 1.2)}$$

Next, choosing an upper and lower strain rate and corresponding stress level from the experimental data, we can write two equations and two unknowns as follows

$$Ln(5.0\times10^{-6}) = Ln\ \gamma_c + \beta\ Ln(125.0) \qquad \text{(A 1.3)}$$

$$Ln(1.0\times10^{-9}) = Ln\ \gamma_c + \beta\ Ln(55.0) \qquad \text{(A 1.4)}$$

Solving these two equations simultaneously we then obtain the values

$$\beta = 10.3747$$

$$\gamma_c = \frac{8.7953\times10^{-28}}{KSI^{10.3747} - sec}$$

Note the units in the denominator, the 10.37468 is required since the stress value is raise o the β power, see equation A 1.1
These units in psi are

$$\beta = 10.3747$$

$$\gamma_c = \frac{8.5796\times10^{-58}}{psi^{10.3747} - sec}$$

APPENDIX B

DETERMINATION OF THE COUPLED MALVERN MATERIAL PARAMETERS.

The exponential law of the Malvern model can be expressed uniaxially by

$$\dot{\epsilon}^{P} = \gamma_p \left\{ \exp\left(\frac{\sigma - \bar{\sigma}}{a}\right) - 1 \right\} \qquad \text{(B 2.1)}$$

If one divides the above equation by γ_p and then takes the natural logarithm of both sides, the equation takes the form

$$\ln \frac{\dot{\epsilon}^{P}}{\gamma_p} = \left(\frac{\sigma - \bar{\sigma}}{a} \right) \qquad \text{(B 2.2)}$$

The above form looks very much like the equation for a straight line, where the γ_p parameter can be thought of as the intercept and the a as the slope.

Since the coupled exponential Malvern is fitted to the higher sloped (viscoplastic strain rates) experimental curve, we then choose upper and lower strain rates on this curve.

Stress (KSI)	Strain Rate (sec^{-1})
180	5.0×10^{-2}
125	5.0×10^{-6}

Substituting the above values into equation B2.2 we can determine the value

$$\ln(10^4) = \left(\frac{55}{a}\right)$$

$$\text{therefore,} \quad a = 5.9716$$

Now the γ_p value can be determined directly, since the a is fixed. Hence, by choosing an $\dot{\epsilon}^p$ and a corresponding overstress value, the γ_p can be determined.

Thus, one can observe how the a value can effect the strain-rate sensitivity of the material since it expresses the slope of the strain rate versus stress curve.

VITA

Michael H. Bohun was born on 16 November, 1954, at Paw Paw, Michigan. He graduated from Schoolcraft High School in Schoolcraft, Michigan, in 1972. He then attended Kalamazoo Valley Community College in Kalamazoo, Michigan and graduated in June 1974, with an Associates degree in Science. Continuing on to Purdue University, he graduated with a B.S. in Aeronautical and Astronautical Engineering in May 1977, and concurrently received his commission as a 2nd lieutenant in the United States Air Force. He then went on to attend a six month Aircraft Maintenance Officer School at Chanute Air Force Base at Rantoul, Illinois. After this training, he was assigned to the 463rd Tactical Airlift Wing in Abilene, Texas. There he performed duties as a Flightline Maintenance Officer and Chief of the Support Equipment Branch from 13 February 1978, to 1 May 1980. While stationed at Dyess Air Force Base, he became a fully qualified maintenance officer and then was selected to attend AFIT'S graduate school of engineering. He is currently being assigned to the Air Force Materials Laboratory, Metals and Ceramics Division, to perform research on aircraft turbine disks for the Air Force Retirement-For-Cause Program.

SECURITY CLASSIFICATION OF THIS PAGE (When Data Entered)

REPORT DOCUMENTATION PAGE		READ INSTRUCTIONS BEFORE COMPLETING FORM
1. REPORT NUMBER AFIT/GAE/AA/81D-4	2. GOVT ACCESSION NO.	3. RECIPIENT'S CATALOG NUMBER
4. TITLE (and Subtitle) High Temperature Viscoplastic and Creep Crack Growth Behavior of IN-100		5. TYPE OF REPORT & PERIOD COVERED MS Thesis 6. PERFORMING ORG. REPORT NUMBER
7. AUTHOR(s) Micahael H. Bohun Captain USAF		8. CONTRACT OR GRANT NUMBER(s)
9. PERFORMING ORGANIZATION NAME AND ADDRESS		10. PROGRAM ELEMENT, PROJECT, TASK AREA & WORK UNIT NUMBERS 77
11. CONTROLLING OFFICE NAME AND ADDRESS		12. REPORT DATE December 1981 13. NUMBER OF PAGES
14. MONITORING AGENCY NAME & ADDRESS(if different from Controlling Office)		15. SECURITY CLASS. (of this report) Unclassified 15a. DECLASSIFICATION DOWNGRADING SCHEDULE

16. DISTRIBUTION STATEMENT (of this Report)

Approved for public release; distribution unlimited

17. DISTRIBUTION STATEMENT (of the abstract entered in Block 20, if different from Report)

18. SUPPLEMENTARY NOTES

28 JAN 1982

Approved for public release; IAW AFR 190-17

FREDERIC C. LYNCH, Major, USAF
Director of Public Affairs

19. KEY WORDS (Continue on reverse side if necessary and identify by block number)

Viscoplasticity	Crack Growth
Creep	Turbine Disks
Time Dependency	Finite Element Modeling
Bodner-Partom Flow Law	Hybrid-Experimental-Numerical Procedure
Malvern-Norton Flow Law	

20. ABSTRACT (Continue on reverse side if necessary and identify by block number)

IN-100, a nickel based powdered alloy, is presently used in turbine disks within the F-100 turbofan engine. It has been found that time dependent inelastic strains can be developed within this material at the high temperature environment of the turbine engine. Previous work performed by Terry D. Hinnerichs involved developing a computer program that would predict crack growth with viscoplastic flow. A large portion of his work used a strain-rate sensitive model known as the Bodner-Partom flow law. Crack growth predictions using this flow law were very encouraging,

DD FORM 1 JAN 73 1473 EDITION OF 1 NOV 65 IS OBSOLETE

SECURITY CLASSIFICATION OF THIS PAGE (When Data Entered)

but the determination of the nine material parameters involved in the flow law presents some difficulties. Therefore, it has been proposed that a much simplified version of a strain-rate sensitive model be employed to capture viscoplastic action.

Hence, this thesis involves the study of various mathematical forms of the Malvern overstress constitutive equation. Each of these models employed a finite element computer program to predict crack growth. The computer program incorporates the constant strain triangles. The residual force method was utilized to handle variations in material stiffness due to plastic deformations and creep. In addition, a Hybrid Experimental-Numerical (HEN) procedure was used to trace crack opening displacements near the crack tip. This HEN procedure insures the model is following the experimental displacement rates accurately. Thus, the crack growth predictions are a by-product of both the rate-sensitive model and near field displacement rates.

The various mathematical representations of the Malvern model were compared to the Bodner-Partom response. Comparisons were made utilizing total plastic work generated, crack growth rates, and effective stress contours and stress profiles.

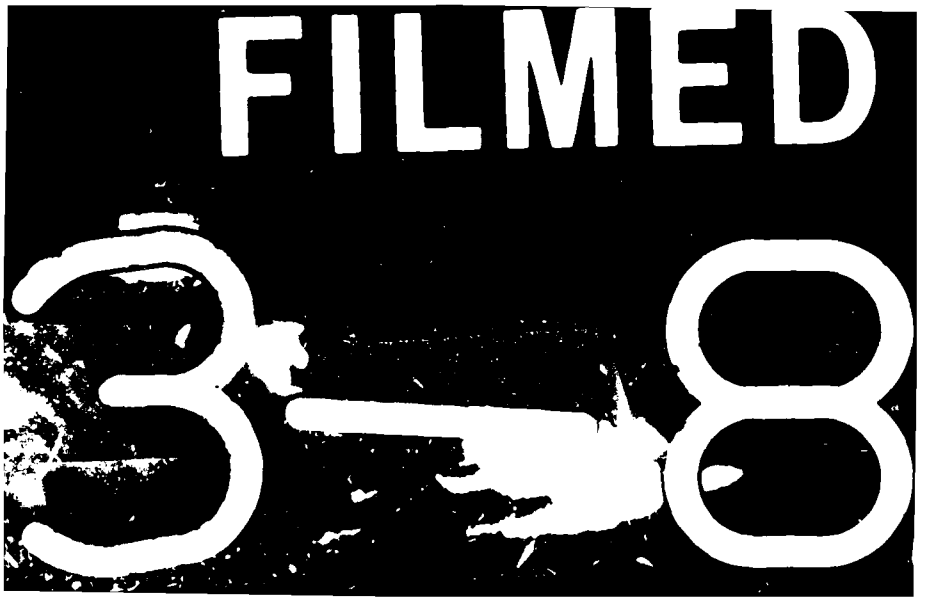
FILMED
3 8